Combining top-down and bottom-up approaches to evaluate recent trends and seasonal patterns in U.K. N_2O emissions

Eric Saboya[1], Alistair J. Manning[2], Peter Levy[3], Kieran M. Stanley[4], Joseph Pitt[4], Dickon Young[4], Daniel Say[4], Aoife Grant[4], Tim Arnold[5,6], Chris Rennick[5], Sam J. Tomlinson[7], Edward J. Carnell[3], Yuri Artoli[8], Ann Stavart[9], T. Gerard Spain[10], Simon O'Doherty[4], Matthew Rigby[4], Anita L. Ganesan[1]

[1]School of Geographical Sciences, University of Bristol, Bristol, U.K.
[2]Met Office Hadley Centre, Exeter, U.K.
[3]U.K. Centre for Ecology and Hydrology, Edinburgh, U.K.
[4]School of Chemistry, University of Bristol, Bristol, U.K.
[5]National Physical Laboratory, Teddington, U.K.
[6]School of GeoSciences, University of Edinburgh, Edinburgh, U.K.
[7]U.K. Centre for Ecology and Hydrology, Lancaster, U.K.
[8]Plymouth Marine Laboratory, Plymouth, U.K.
[9]Climate Science Centre, CSIRO Oceans and Atmosphere, Aspendale, Australia
[10]School of Natural Sciences, University of Galway, Galway, Ireland

Key Points:

- Atmospheric N_2O measurements from 2013-2022 are used to evaluate the U.K.'s reported emissions using two inverse methods.
- Emissions derived from atmospheric data are on average $14 - 33\%$ higher than the U.K.'s national emissions inventory values across 2013-2022.
- Agreement between the average top-down and bottom-up seasonal emissions was improved by decreasing bottom-up synthetic fertilizer emissions

Corresponding author: Eric Saboya, eric.saboya@bristol.ac.uk

Corresponding author: Anita Ganesan, anita.ganesan@bristol.ac.uk

Abstract

Atmospheric trace gas measurements can be used to independently assess national greenhouse gas inventories through inverse modelling. Here, atmospheric nitrous oxide (N_2O) measurements made in the United Kingdom (U.K.) and Republic of Ireland are used to derive monthly N_2O emissions for 2013-2022 using two different inverse methods. We find mean U.K. emissions of 90.5 ± 23.0 (1σ) and 111.7 ± 32.1 (1σ) Gg N_2O yr^{-1} for 2013-2022, and corresponding trends of -0.68 ± 0.48 (1σ) Gg N_2O yr^{-2} and -2.10 ± 0.72 (1σ) Gg N_2O yr^{-2}, respectively for the two inverse methods. The U.K. National Atmospheric Emissions Inventory (NAEI) reported mean N_2O emissions of 73.9 Gg N_2O yr^{-1} across this period, which is 14−33% smaller than the emissions derived from atmospheric data. We infer a pronounced seasonal cycle in N_2O emissions, with a peak occurring in the spring and a second smaller peak in the late summer for certain years. The springtime peak has a long seasonal decline that contrasts with the sharp rise and fall of N_2O emissions estimated from the bottom-up U.K. Emissions Model (UKEM). Bayesian inference is used to minimize the seasonal cycle mismatch between the average top-down (atmospheric data-based) and bottom-up (process model and inventory-based) seasonal emissions at a sub-sector level. Increasing agricultural manure management and decreasing synthetic fertilizer N_2O emissions reduces some of the discrepancy between the average top-down and bottom-up seasonal cycles. Other possibilities could also explain these discrepancies, such as missing emissions from NH_3 deposition, but these require further investigation.

1 Introduction

Atmospheric nitrous oxide (N_2O) is an important, long-lived greenhouse gas (GHG) that also contributes to the depletion of stratospheric ozone. Whilst global emissions of N_2O are well-constrained at around 17 Tg N_2O yr^{-1} (Stell et al., 2022; Tian et al., 2020; Thompson et al., 2019; Wells et al., 2018) there are significant regional-scale differences between top-down (based on atmospheric data) and bottom-up (based on process models and/or inventories) N_2O emissions estimates (e.g. Wells et al., 2018; Jeong et al., 2018; Thompson et al., 2014).

The United Kingdom's bottom-up N_2O emissions are reported in the U.K. National Atmospheric Emissions Inventory (NAEI; Ricardo Energy & Environment, 2019) each year which inform the National Inventory Reports (NIRs) submitted annually to the United Nations Framework Convention on Climate Change (UNFCCC). Anthropogenic emissions of N_2O are reported to be 72.6 Gg N_2O yr^{-1} for the year 2021 (Brown et al., 2023), which are around 4% of the U.K.'s total carbon dioxide equivalent ($CO_{2,eq}$) GHG emissions. Agricultural N_2O emissions in the reported inventory account for 70% of 2021 U.K. N_2O emissions, with $\sim 10\%$ of U.K. N_2O emissions attributed to fossil fuel combustion and fugitive emissions, and the remaining anthropogenic emissions coming from the waste and industrial sectors (Fig. 1; Brown et al., 2023). Agricultural emissions are predominately from agricultural soils (57% of U.K. N_2O emissions) with the remaining agricultural N_2O emissions mostly from livestock manure management as well as indirect emissions from nitrogen runoff and leaching. A feature of the NAEI is that GHG fluxes are spatially distributed at 1 km^2 resolution for each SNAP (Selected Nomenclature for reporting of Air Pollutants) sector.

Under the 2008 Climate Change Act (UK Government, 2008) the U.K. has ambitious goals to achieve net-zero GHG emissions by 2050. Interim targets ("Carbon Budgets") have been enacted, with the Fifth U.K. Carbon Budget requiring GHG emissions to be reduced to 57% of 1990 $CO_{2,eq}$ levels by 2030 (Committee on Climate Change, 2015). Current GHG emissions mitigation policy suggest U.K. N_2O emissions will remain approximately constant until 2030 (U.K. Department for Energy Security and Net Zero,

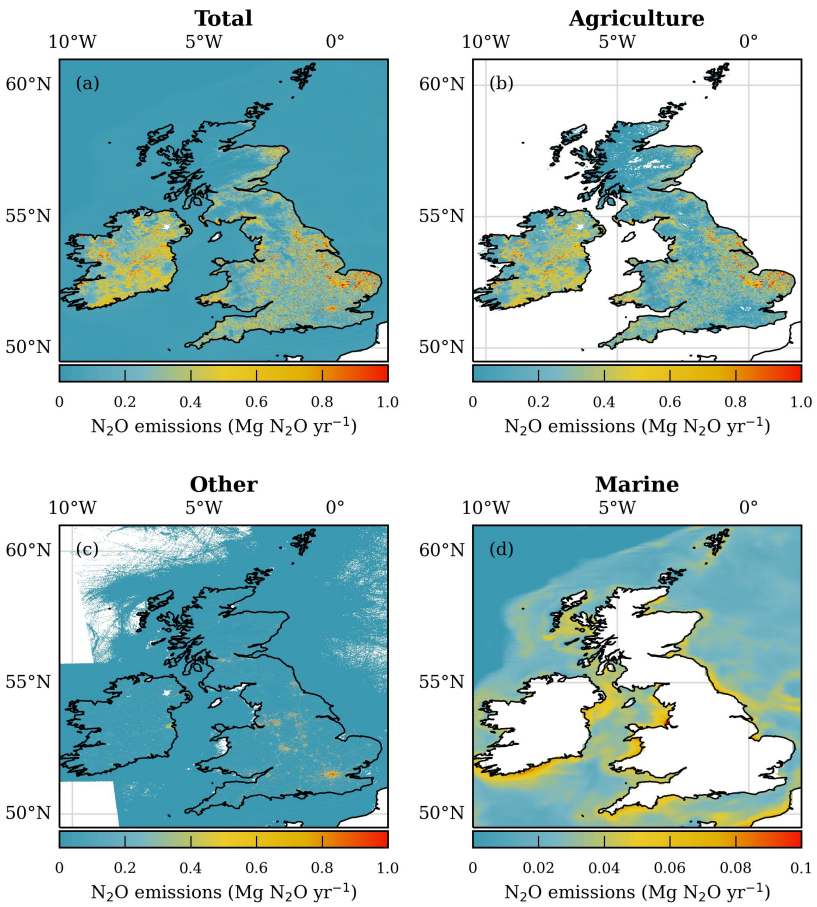

Figure 1. Bottom-up UKEM (a) total; (b) agricultural; (c) other anthropogenic (including shipping); (d) marine N_2O emissions for the year 2020 at 1 km^2 spatial resolution. Note that marine emissions are on a smaller scale than the other sectors and are not part of the NAEI. White areas indicate where emissions are zero.

2022). Given the potential uncertainties in inventories, which are used to guide these policy scenarios, there is a need to independently monitor progress towards such targets.

Atmospheric mole fraction measurements of trace gases can be used to evaluate emissions reported in national greenhouse gas inventories through inverse modelling. Atmospheric measurements are used in the inverse model to adjust bottom-up emissions through Bayesian inference. This approach has previously been used for deriving top-down N_2O emissions estimates for the U.K. (Manning et al., 2011; Ganesan et al., 2015) and elsewhere (e.g. Stell et al., 2022; Nevison et al., 2018; Thompson et al., 2014). Previous studies found top-down emissions were approximately $13-22\%$ lower than those reported in the U.K. inventory at that time (Manning et al., 2011; Ganesan et al., 2015). Top-down estimates for earlier than 2012 had relatively large uncertainties as atmospheric observations were only available from the Mace Head station on the west coast of the Republic of Ireland (Fig. 2). The establishment of the U.K. Deriving Emissions linked to Climate Change (DECC) network in 2012 for making continuous measurements of atmospheric trace gases across the U.K. (Stanley et al., 2018; Stavert et al., 2019) has improved top-down emissions estimates, providing a higher sensitivity to emissions across

the U.K. and Republic of Ireland, leading to smaller top-down uncertainties (e.g. Lunt et al., 2021).

Ganesan et al. (2015), using atmospheric N_2O measurements from the U.K. DECC network with a hierarchical Bayesian inverse model (Ganesan et al., 2014), found average U.K. emissions of 101 (68-150) Gg N_2O yr^{-1} for 2012-2014 and identified a pronounced seasonal cycle with an amplitude of $\sim$ 50 Gg N_2O yr^{-1} peaking during the early summer. The observed seasonality was hypothesized to be due to agricultural application of nitrogen-based fertilizers.

Seasonal changes in U.K. N_2O emissions are not captured in the U.K. NAEI inventory, which only produces annual estimates. To facilitate comparison of top-down and bottom-up seasonal cycles, temporal profiles derived from direct flux measurements and other data sources are used to downscale the annual NAEI N_2O emissions at a source sub-sector level to a monthly time resolution and combined with marine emissions from Lessin et al. (2020) for the surrounding seas in the U.K. Emissions Model (UKEM, previously referred to as "UKGHG") (P. Levy, 2020).

Here, we present results of top-down U.K. N_2O emissions from 2013-2022 derived using two different Bayesian inverse models and compare these estimates to the U.K. NAEI and the downscaled monthly estimates from the UKEM. Compared to previous U.K. N_2O publications, we use observations from five stations in the U.K. DECC network (only three stations were available for Ganesan et al. (2015)) and over a longer time period, resulting in better resolved emission trends and seasonal patterns.

2 Data and Methods

2.1 Atmospheric measurements

We use atmospheric N_2O mole fraction measurements from five U.K. DECC network stations (Stanley et al., 2018; Stavert et al., 2019) between 2013-2022. Tall-tower measurement stations in the U.K. DECC network sample ambient air from inlets mounted $>$ 90 m above ground level (agl) on telecommunications towers (Fig. 2), and the coastal Mace Head (MHD) station measures closer to the surface at $\sim$ 10 m agl. Atmospheric N_2O measurements from MHD, Tacolneston (TAC) and Ridge Hill (RGL) stations sampled across the entire 2013-2022 period, with Bilsdale (BSD) and Heathfield (HFD) becoming operational in 2014.

Both gas chromatograph coupled to electron capture detectors (GC-ECD) and optical-based instruments (Picarro G5310, LGR; Text S1) are used for measuring atmospheric N_2O mole fractions in the U.K. DECC network. Optical instruments are calibrated to the World Meteorological Organization (WMO)-X2006A scale (Hall et al., 2007) with samples averaged into $\sim$ 1 min intervals. The GC-ECD instruments are calibrated to the Scripps Institution of Oceanography (SIO-16) scale and sample approximately every 10 min. A correction of -0.43 ppb is applied to N_2O measurements made on the SIO-16 scale to adjust these measurements to the WMO-X2006A calibration scale (Prinn et al., 2018).

At certain measurement stations (e.g. BSD) there are periods when concurrent GC-ECD and optical-based atmospheric N_2O measurements are available. In such cases, we use measurements from optical-based instruments in preference to those from the GC-ECD instruments, due to their greater precision and higher frequency. Measurements are always used from the highest air inlet available. Information about the instrumentation and inlet heights used for each of the stations are summarized in Fig. 2, with the U.K. DECC network further described in Stanley et al. (2018) and Stavert et al. (2019).

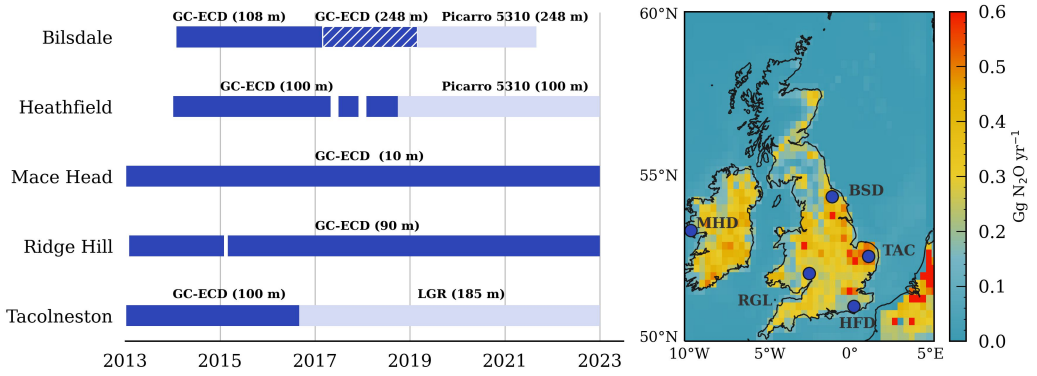

Figure 2. Summary of atmospheric N_2O mole fraction data used from the U.K. DECC network for 2013-2022. Instrument names and inlet heights (in brackets with "m" referring to metres above ground level) used for different periods are shown on the left. Gaps (white space) denote when measurements were unavailable. Shaded blue sections represent when gas chromatographs coupled to electron capture detectors (GC-ECD) were used, whereas sections shaded in lighter blue are when optical spectrometers were used. Hashed areas represent periods using GC-ECD measurements after a change in inlet height. Station locations are shown on the right in blue along with the May 2020 UKEM N_2O emissions regridded to match the NAME footprint resolution.

Measurements were averaged over 4 h periods and filtered to remove measurements that are more likely to be affected by local processes during times of stagnant air (e.g. Ganesan et al., 2015). Such meteorological conditions are unlikely to be accurately captured at the spatiotemporal resolution of the atmospheric transport model (Section 2.2) used in this work. Each inverse model uses a different approach for filtering atmospheric measurements during stagnant air conditions. Further details about the filtering approaches are provided in Text S2. A comparison of top-down emissions derived using the same inverse method but with the different filtering approaches, and without any data filtering, is presented in Text S3.

Uncertainty in the atmospheric N_2O observations is quantified as the sum in quadrature of the instrument precision and observation variability in the 4 h averaging period. Observation uncertainties were on average ~ 0.28 ppb for the GC-ECD instruments and ~ 0.21 ppb for the optical instruments across the respective periods shown in Fig. 2.

2.2 Atmospheric transport model

The U.K. Met Office Lagrangian dispersion model: NAME (Numerical Atmospheric dispersion Modelling Environment; Jones et al., 2007) v7.2 was used to quantify the relationship between surface emissions and atmospheric mole fractions observed at each measurement station in both inverse models (Section 2.3). "Footprints" of surface emission sensitivities were calculated from ensembles of particle back-trajectories in NAME. Each grid cell of the footprint describes the influence of emissions from that grid cell on the mole fraction measured at the receptor site at a certain time (Manning et al., 2011; Rigby et al., 2012).

Here, NAME footprints use the same specification as Manning et al. (2021). Hourly footprints were calculated with a $\sim$ 25 km ($0.352^o \times 0.234^o$) spatial resolution over a model domain spanning approximately 98^o W to 40^o E and 11^o N to 79^o N using a 30-

day back-trajectory duration and particle release rate of 2×10^4 h^{-1}. Meteorological fields from the Met Office Unified Model (UM) underlie the footprints with hourly, high-resolution up to $\sim$ 1.5 km ($0.0135^o \times 0.0135^o$) with 57 vertical levels up to $\sim$ 12 km UKV meteorological fields used for over the British Isles and 3-hourly UM $0.1406^o \times 0.0938^o$ with 59 vertical levels up to $\sim$ 30 km global meteorological fields used for the rest of the modelling domain.

Footprints were combined with gridded a priori emissions (Section 2.4) to simulate atmospheric N_2O mole fractions at each measurement station.

2.3 Inversion methodology

Two inverse models - InTEM (Inversion Technique for Emissions Modelling) and RHIME (Regional Hierarchical Inverse Modelling Environment) - are used for deriving top-down U.K. N_2O fluxes and are described below. Whilst both inverse models follow a Bayesian framework the inverse methods differ in several aspects: in the calculation of boundary condition/baseline mole fractions; the treatment of model-data uncertainties; and the approach for calculating the posterior emissions. Both inverse models infer emissions for each calendar month assuming N_2O emissions are constant in each 1-month period of inference.

2.3.1 InTEM inverse model

InTEM is an established Bayesian inverse model (Arnold et al., 2018; Manning et al., 2011, 2021) developed by the U.K. Met Office that has been widely used for trace gas inversions of different species across different regions (e.g. Rigby et al., 2019; Manning et al., 2021; Ganesan et al., 2020). InTEM is also used by the U.K. government for evaluating its nationally reported greenhouse gas emissions (Brown et al., 2022, 2023).

The InTEM framework minimizes the model-data mismatch constrained by observation uncertainties, model uncertainties, and a priori information and its associated uncertainties, which are assumed to be Gaussian. To prevent non-physical solutions, InTEM uses a non-negative least squares solver. The model-data uncertainty is calculated as the sum in quadrature of the observational uncertainty, baseline uncertainty and estimated model uncertainty. The model uncertainty forms the largest contribution of the model-data uncertainty in InTEM and is calculated (for all trace gas species) by using the larger of: the concentration of the median pollution event over the year, or 10% of the concentration of the individual pollution event.

InTEM uses gridded N_2O emissions estimates (Section 2.4) and a time-varying mole fraction baseline as a priori constraints. The mole fraction baseline is derived using atmospheric N_2O measurements from Mace Head that are representative of the well-mixed northern hemispheric baseline. This baseline is derived using filters to minimize influences from populated regions, local sources, high altitudes and southerly latitudes (Manning et al., 2021). The mole fraction baseline is subsequently adjusted in the inversion by 11 values depending on the geographical direction and altitude from which the air enters the model domain (Arnold et al., 2018), along with the spatial distribution of N_2O emission values (Manning et al., 2021; Arnold et al., 2018). InTEM solves for posterior emissions in 100 scaling regions across Europe and imposes an a priori emissions uncertainty of 80% of NAEI N_2O emissions for the U.K. To account for small systematic differences in the modelling and between measurements, a prior offset uncertainty with 1σ uncertainty of 0.6 ppb is included for each station and subsequently solved for in the inversion. InTEM is further described in Manning et al. (2021); Arnold et al. (2018); Redington et al. (2023).

2.3.2 RHIME inverse model

RHIME (also previously referred to as "Bristol-MCMC"; Ganesan et al., 2014) has been frequently used for trace gas inversions of various atmospheric species across the globe (e.g. Say et al., 2021; Ganesan et al., 2015; Western et al., 2022). Here, Bayesian inference using MCMC (Markov Chain Monte Carlo) is used to quantify a mean scaling (with confidence intervals) of a priori emissions across 193 scaling regions in the model domain. A scaling of boundary conditions on the four cardinal boundaries of the NAME domain is also derived in the inversion.

Boundary condition fields representing mole fractions along the edges of the model domain are specified using CAMS (Copernicus Atmosphere Monitoring Service) v20r1 global inversion-optimized fluxes for each month. A scaling is calculated for each boundary in each 1-month period of inference to derive posterior boundary condition mole fractions. This ensures the CAMS data are not systematically underestimating or overestimating the baseline mole fractions at each of the measurement stations.

RHIME uses hyperparameters that characterize probability density functions (PDFs) of: the a priori emissions, boundary condition mole fractions, model-data covariances and offset terms. The RHIME framework allows uncertainties in the scaling parameters to be included in the model, with the a priori scaling sampled from a lognormal distribution $\sim LN(\mu = 0.346, \sigma = 0.693)$ and the model-data uncertainty from $\sim LN(\mu = -0.987, \sigma = 0.588)$. The model-data uncertainty is calculated as the sum in quadrature of the observational uncertainty and the absolute model uncertainty - derived from the model-data hyperparameter. The offset term is normally distributed with $\mu = 0$ ppb, $\sigma = 0.60$ ppb. Like Western et al. (2022) and Say et al. (2021), we use a No-U-Turn (NUTS) sampler (Hoffman & Gelman, 2014) for the a priori emissions and a slice sampler for estimating the model-data uncertainty. The samplers used a total 250,000 iterations (discarding the first 50,000) with 2 chains running in parallel. A Gelman-Rubin diagnostic is used to check for parameter convergence in both chains.

2.4 A priori emissions

The UKEM model (P. Levy, 2020) takes spatial data from the U.K. and Republic of Ireland inventories and processes them in a number of steps. These steps include: reprojection to a latitude–longitude grid, combining point- and area-based emissions, reconciling data from different sources into a single consistent classification scheme, rescaling to match national totals, back-projecting a time series of maps as inventories are updated annually, and adding in marine biogenic fluxes. For N_2O, marine biogenic fluxes from NEMO-ERSEM (the Nucleus for European Modelling of the Ocean model coupled with the European Regional Seas Ecosystem Model; Lessin et al., 2020) were used as the best available data on fluxes for the coastal sea around the U.K.

Inventory data are only produced annually. However, emissions may vary over much shorter timescales. The annual-scale emissions are therefore disaggregated in time in UKEM, to give the appropriate seasonal, day-of-week, and diurnal patterns. For some sectors, the variation in time is largely negligible (e.g. industry) or poorly known (e.g. LULUCF, waste), and these are represented as constant in time. For other sectors (agriculture, transport, energy), strong temporal patterns exist and can be characterized with activity data at higher temporal resolution from a variety of sources (P. Levy, 2020).

For N_2O, the key sector is agriculture, and the UKEM model uses activity data from the same process as the agricultural GHG inventory (Brown et al., 2023) but at monthly resolution when available. For example, the timing of synthetic fertilizer application is estimated from the British Survey of Fertiliser Practice (`https://www.gov.uk/government/collections/fertiliser-usage`). The timing of N_2O emission after application is estimated from existing data where fluxes have been measured in the field, generally us-

ing the closed static chamber technique. Typically, most of the emission occurs within only a few weeks of application (P. E. Levy et al., 2017). This produces a pronounced peak in the late spring, closely following the pattern in the application of synthetic fertilizer. The spatial distribution follows the distribution of cropland, where fertilizer inputs are highest (Fig. 1). An additional source is the mineralization of degrading peat soils in the Fenland areas in south-east England, though the magnitude of this is very uncertain.

Emissions from the marine sector are generally highest in the coastal zone, where inputs from rivers produce higher nitrogen concentrations. However, even near the coast, marine emissions are generally around ten times smaller than land emissions (Fig. 1), and although they peak during summer, their influence on the overall pattern is relatively small. At times, the modelled marine fluxes show net N_2O uptake, but only in a small region in the north-west of the domain.

As UKEM N_2O monthly emissions are only available for the U.K. and Republic of Ireland, $0.1^o \times 0.1^o$ monthly anthropogenic emissions from EDGAR (Emissions Database for Global Atmospheric Research; Crippa et al. (2021)) v6.0 are used for the rest of the modelling domain. Version 6.0 is used because monthly N_2O emissions are not currently available in the latest version (v7.0) of EDGAR. We "regrid" emissions data to match the NAME footprint spatial resolution and domain using a mass-conservative approach. As gridded emissions are only available for each month in 2013-2020, 2020 emissions are used as the a priori estimate for the 2021 and 2022 inversions.

Two sets of a priori emissions are used in the inversions. The first uses the monthly-resolved emissions and the second uses annual emissions, which are constant across each year. This provides an additional means of diagnosing whether any seasonal trends in the posterior emissions are driven by atmospheric measurements or by the a priori emissions.

2.5 Optimization of sectoral seasonal profiles

We are interested in comparing the U.K. top-down (derived using the inverse models; Section 2.3) and bottom-up (modelled in UKEM; Section 2.4) seasonal emissions profiles.

To investigate which N_2O emission sources could be driving seasonal differences we identified key agricultural sub-sectors that exhibit seasonal cycles in the U.K. These are: synthetic fertilizer usage, and manure management practices relating to: cattle during times they are housed ("cattle housing"), cattle during times of grazing ("cattle grazing"), the spreading of cattle manure, the spreading of poultry manure, and the spreading of digestate. Bottom-up emissions from all remaining N_2O sources are aggregated together. Each of these sub-sectors has a distinct temporal seasonal profile in the bottom-up UKEM emissions.

Here, we optimize the 2013-2022 averaged UKEM sub-sector emissions profiles to the averaged top-down seasonal emissions cycles - derived using InTEM and RHIME - to investigate which bottom-up emissions sources could be leading to differences with the top-down seasonal cycles.

We use a Bayesian approach to calculate the scale factors for each bottom-up sub-sector that minimizes the mismatch with the average top-down seasonal cycles. The posterior scale factors, $\mathbf{X}_{post}$, for each of the seven bottom-up sub-sector seasonal profiles are calculated using:

$$\mathbf{X}_{post} = \mathbf{X}_{prior} + (\mathbf{Q}_{prior}\mathbf{H}^{\mathbf{T}})(\mathbf{H}\mathbf{Q}_{prior}\mathbf{H}^{\mathbf{T}} + \mathbf{R})^{-1}(\mathbf{Y} - \mathbf{H}\mathbf{X}_{prior}), \quad (1)$$

with associated covariance:

$$\mathbf{Q}_{post} = \mathbf{Q}_{prior} - (\mathbf{Q}_{prior}\mathbf{H}^{\mathbf{T}})(\mathbf{H}\mathbf{Q}_{prior}\mathbf{H}^{\mathbf{T}} + \mathbf{R})^{-1}\mathbf{H}\mathbf{Q}_{prior}. \quad (2)$$

Here, $\mathbf{X}_{prior}$ is a 7×1 matrix with elements of value 1 denoting the a priori scale factors for each UKEM emissions sub-sector. $\mathbf{H}$ is a 12×7 matrix representing the monthly sub-sector UKEM seasonal emissions profiles (in Gg N_2O yr^{-1}). $\mathbf{Y}$ is a 12×1 matrix representing the average top-down seasonal emissions (in Gg N_2O yr^{-1}) with associated uncertainties (in Gg N_2O yr^{-1}) captured in $\mathbf{R}$. Matrix $\mathbf{R}$ is a 12×12 diagonal matrix where each element is the corresponding monthly 1σ value of the top-down seasonal emissions cycle. The uncertainty of the scale factors for each of the UKEM seasonal profiles are captured in $\mathbf{Q}$ which is a 7×7 diagonal matrix with elements of value 1 denoting uncertainties of 100% on each of the bottom-up sub-sectors.

3 Results

3.1 Emissions and trends in N_2O (2013-2022)

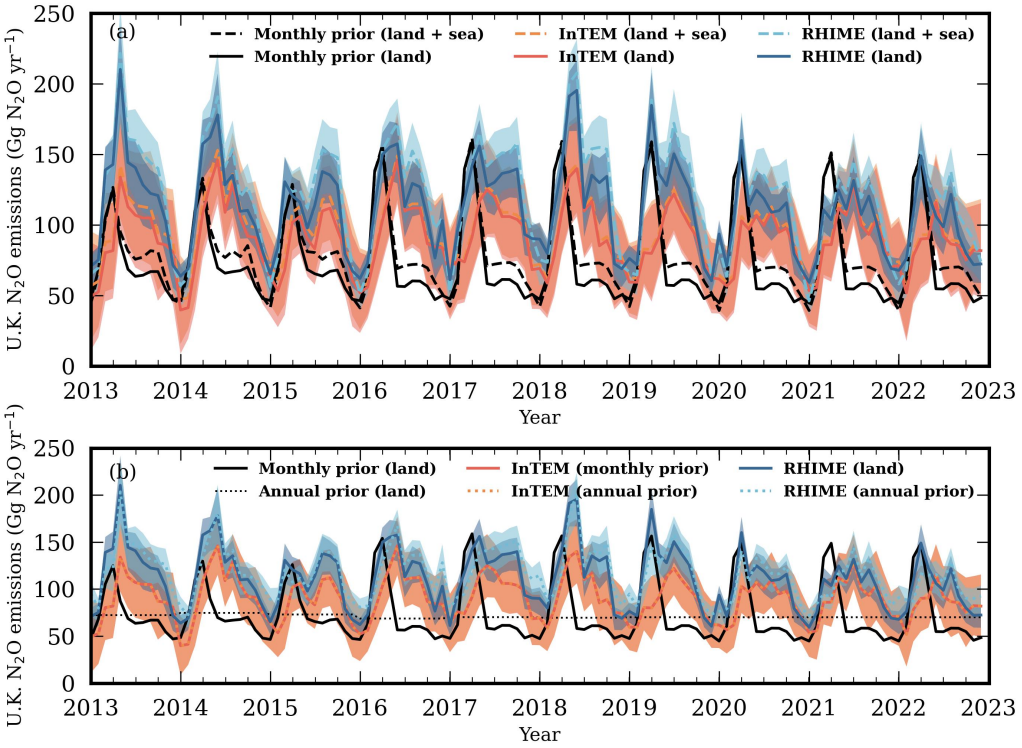

Figure 3. Time series of a priori and posterior monthly N_2O emissions for the U.K. (a) Mean monthly posterior emissions from InTEM (red) and RHIME (blue) for the land component of the U.K. (solid line) and the land plus surrounding seas of the U.K. (dashed line) with corresponding monthly a priori emissions in black. (b) InTEM and RHIME posterior emissions derived using monthly varying a priori emissions (solid line) and annually constant a priori emissions (dotted line). Shaded regions correspond to the 68% confidence interval ranges in both panels.

Top-down U.K. N_2O emissions were generally higher than their corresponding bottom-up UKEM/NAEI emissions across the 10-year period spanning January 2013 to December 2022 (Fig. 3, Table 1). On average, top-down emissions from RHIME were 38.0±

32.6(1σ) Gg N_2O yr^{-1} (32.7%) higher than the bottom-up estimates, and InTEM was $16.8 \pm 37.4\,(1\sigma)$ Gg N_2O yr^{-1} (14.0%) higher. Whilst RHIME posterior emissions are on average $21.2 \pm 19.9\,(1\sigma)$ Gg N_2O yr^{-1} higher than the InTEM posterior emissions, there are overlapping 68% confidence intervals (CI) for most of the inversion period. The InTEM and RHIME top-down emissions are statistically well-correlated ($R^2 = 0.86$, $p < 0.01$). We later discuss potential reasons for differences between the InTEM and RHIME top-down emissions (Section 4).

We find an average of 5% of U.K. top-down emissions originate from the surrounding seas (Fig. 3a; Table 1), whereas a priori emissions estimate 8% of U.K. N_2O emissions arise from the marine sector. InTEM infers that marine emissions should on average be lower than the bottom-up estimates whereas RHIME infers the opposite (Table 1). Previous studies have highlighted that U.K. DECC stations are less sensitive to offshore emissions (Lunt et al., 2021) and as marine emissions form a small proportion of U.K. N_2O emissions we therefore limit our analysis to land-based emissions.

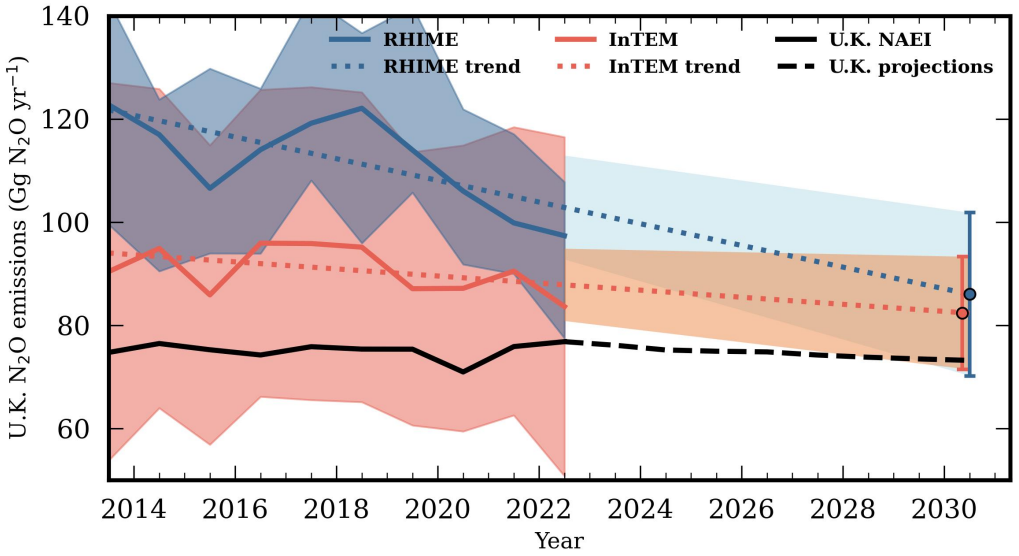

Figure 4. Annual top-down U.K. N_2O emissions from InTEM (red) and RHIME (blue) along with the linear trends for 2013-2022 that are extrapolated to 2030, with 2030 values indicated by circular markers. Shaded areas and error bars denote the 1σ range. Current U.K. NAEI emissions and U.K. DESNZ projected emissions are shown in black.

We determine the RHIME and InTEM emissions trend over 2013-2022 by applying a linear regression to the annual totals. Across this period, a mean negative trend of $-2.10 \pm 0.72 (1\sigma)$ Gg N_2O yr^{-2} ($p < 0.01$) was calculated for RHIME top-down emissions and -0.68 ± 0.48 (1σ) Gg N_2O yr^{-2} ($p < 0.01$) for InTEM top-down emissions (Fig. 4). Figure 4 shows that, comparatively, the NAEI N_2O emissions remain relatively constant across this period.

The U.K. Government Department for Energy Security and Net Zero (DESNZ) produces GHG emissions projections based on current U.K. NAEI emissions and existing/near-finalised U.K. emissions mitigation policies (UK Department for Business Energy and Industrial Strategy, 2022). Projected U.K. N_2O emissions from 2022-2030 are shown in Fig. 4 and remain relatively constant at around 70 Gg N_2O yr^{-1}. Extrapolating the InTEM and RHIME 2013-2022 emissions trends finds projected emissions of $82.3 \pm 10.9 (1\sigma)$

Table 1. Summary of 2013-2022 mean U.K. posterior and a priori N_2O emissions and their differences reported with 1σ uncertainty. "Monthly" and "Annual" reference posterior emissions derived using the monthly and annual UKEM emissions, respectively.

Inversion	InTEM		RHIME		UKEM
setup	Monthly	Annual	Monthly	Annual	Monthly
Land emissions (Gg N_2O yr^{-1})	90.5 ± 23.0	90.5 ± 23.0	111.7 ± 32.1	116.1 ± 26.9	73.7 ± 31.9
Marine emissions (Gg N_2O yr^{-1})	4.2 ± 2.1	4.2 ± 2.2	8.1 ± 10.5	17.9 ± 29.9	6.4 ± 6.9
Land plus marine emissions (Gg N_2O yr^{-1})	94.7 ± 23.1	94.7 ± 23.0	119.8 ± 37.1	129.7 ± 36.0	80.1 ± 30.8
	Mean Posterior - A Priori Emissions				
Land					
Percentage difference	$14.0 \pm 41.0\%$	$9.1 \pm 41.0\%$	$32.7 \pm 23.2\%$	$30.7 \pm 15.5\%$	-
Gg N_2O yr^{-1} difference	16.8 ± 37.4	14.1 ± 22.9	38.0 ± 32.6	39.7 ± 26.5	-
Marine					
Percentage difference	$-87.3 \pm 230.4\%$	$-120.0 \pm 74.4\%$	$29.6 \pm 18.9\%$	$23.7 \pm 16.1\%$	-
Gg N_2O yr^{-1} difference	-2.2 ± 7.2	-3.4 ± 1.9	1.7 ± 4.3	5.9 ± 27.8	-
Land plus marine					
Percentage difference	$12.7 \pm 35.4\%$	$5.3 \pm 25.8\%$	$30.7 \pm 22.5\%$	$31.5 \pm 14.9\%$	-
Gg N_2O yr^{-1} difference	14.6 ± 33.4	10.6 ± 22.9	39.7 ± 34.4	31.5 ± 14.9	-

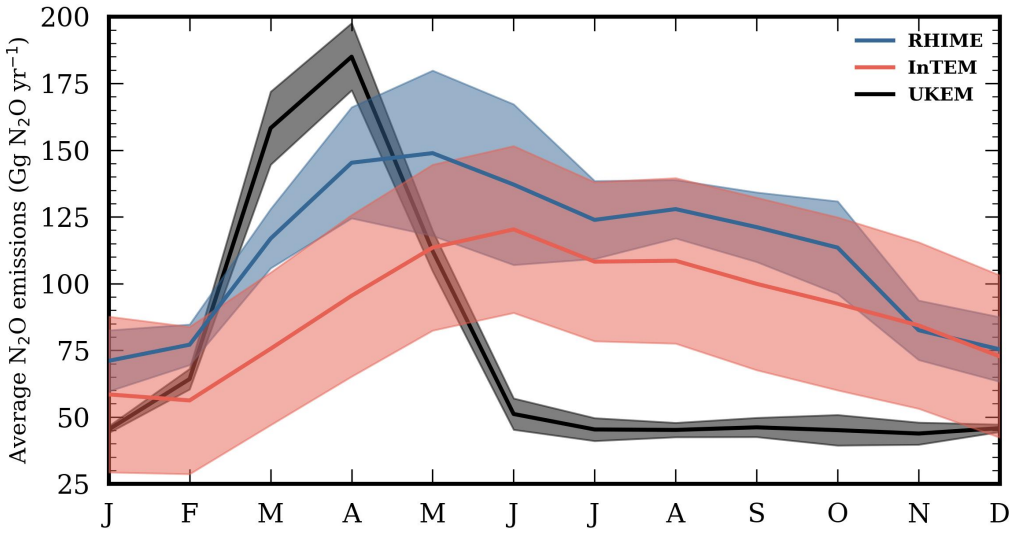

Figure 5. Average seasonal emissions profile across 2013-2022 with shaded regions denoting the 1σ standard deviation in emissions for each month.

Gg N_2O yr^{-1} and 86.5 ± 16.7 (1σ) Gg N_2O yr^{-1}, respectively, for the year 2030 (Fig. 4).

3.2 Seasonal cycles

Pronounced seasonal cycles are observed in the top-down emissions with seasonal highs occurring during the summer and seasonal lows during the winter (Fig. 5). We find these seasonal cycles are insensitive to the seasonality in the prior. Fig. 3b shows a comparison between posterior emissions that used a priori monthly UKEM emissions that either included or excluded a seasonal cycle. A pronounced seasonal peak is always derived in the top-down emissions, and there is strong agreement between the two sets of posterior emissions (Table 1), indicating that the derived seasonal cycle is primarily observation driven.

In certain years there is a clearly identifiable springtime peak, as modelled in the bottom-up UKEM emissions, and a secondary, smaller peak occurring later in the year. From 2020 onwards these two seasonal peaks are less distinct in the top-down emissions compared to earlier years (Fig. 3).

The average seasonal emissions from 2013-2022 for top-down and bottom-up emissions are shown in Fig. 5. In UKEM, the modelled springtime seasonal peak rapidly declines. This is not seen in the top-down emissions, which instead fall more slowly. Additionally, the secondary peak that is sometimes seen in the top-down emissions seasonal cycles (Fig. 3) is not seen in UKEM. We find there are differences between the average InTEM and RHIME seasonal cycles. Notably, the occurrence of a late-summer/autumnal peak is less distinctive in InTEM than in RHIME, with the average InTEM seasonal cycle appearing more prolonged. The shaded regions in Fig. 5, which denote the 1σ standard deviation in emissions for each month across 2013-2022, indicate variability in the RHIME seasonal cycle is generally lower than in InTEM for most months. Where the variability in the InTEM cycle is similar each month (Fig. 5), the variability in the RHIME seasonal cycle between April-July, when the seasonal maximum occurs, is much larger than in other months.

3.3 Uncertainty analysis

Median RHIME and InTEM model-data uncertainties with their 68% confidence intervals for each station are shown in Fig. 6a. Whilst median model-data uncertainties are less than 1 ppb, InTEM uncertainties are nearly four times larger than those from RHIME. These differences are reflected in the 68% CI uncertainty ranges of top-down emissions which are generally larger in InTEM. Whilst differences in model-data uncertainties could be partially attributed to the different inversion frameworks, it highlights the need for using different inverse methods that describe model-data uncertainties in different ways to ensure top-down emissions are more fully understood.

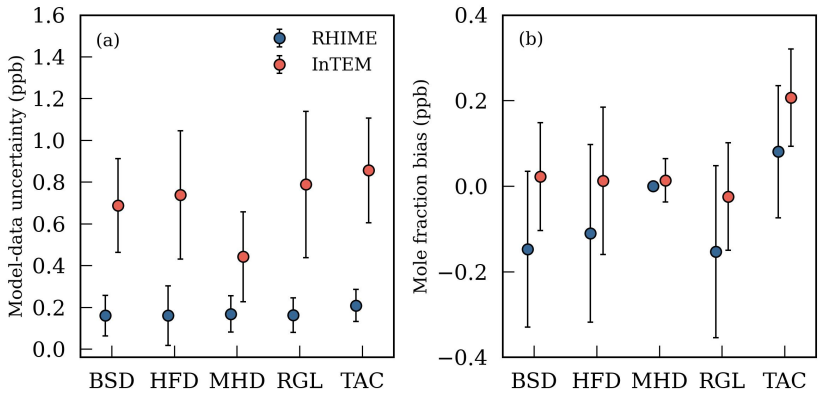

Figure 6. (a) Mean model-data uncertainties for InTEM (red) and RHIME (blue) for each of the measurement stations with error bars denoting the 68% confidence intervals. (b) Inverse model posterior offset bias median and 68% confidence intervals for each of the stations calculated in InTEM (red) and RHIME (blue).

The InTEM and RHIME inversions account for any small instrumental (or model-related) differences that might occur in the atmospheric measurements across the network by solving for a mole fraction bias at each measurement station in each month. The median values with their 68% confidence intervals for each measurement station in InTEM and in RHIME are shown in Fig. 6b. The median bias values from each inversion are typically within ±0.2 ppb at each station; similar to the measurement precision of the instruments (Section 2.1). However, median values differ by around 0.1 ppb between InTEM and RHIME with the largest discrepancies occurring at Bilsdale and Ridge Hill stations. The large, overlapping 68% confidence intervals indicate considerable variability in the biases that are solved in the monthly inversions. The posterior biases underscore that instrument or model-related differences exist across the U.K. DECC network at a magnitude comparable to the measurement uncertainty for N_2O. The high-variability in the calculated bias values suggests that these instrument-related differences are not constant in time and should be accounted for in N_2O inverse modelling studies using measurements from the U.K. DECC network (Thompson et al., 2011, 2014).

3.4 Posterior UKEM sub-sector emissions seasonal profiles

Figure 7a shows the 2013-2022 averaged UKEM seasonal cycles of six N_2O agricultural emissions sub-sectors (Section 2.5) with the remaining land-based N_2O emissions aggregated under “Other”. The pronounced springtime peak is driven by synthetic fertilizer emissions with some contribution from the manure management sub-sectors.

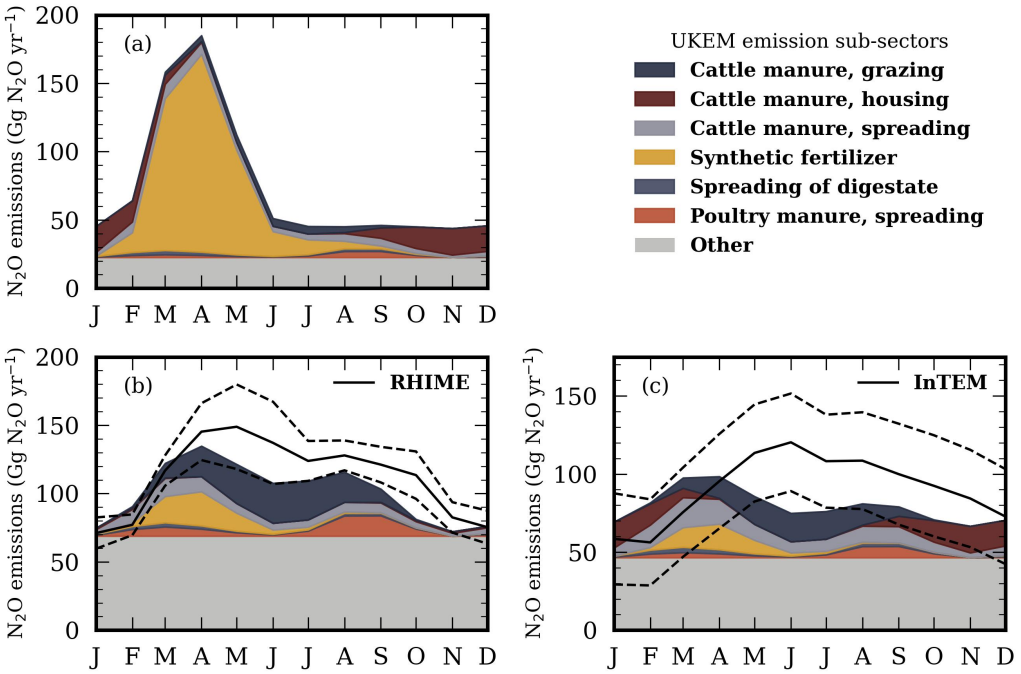

Figure 7. 2013-2022 average N_2O seasonal emissions profiles. (a) Disaggregated sub-sector emissions profiles as modelled in UKEM. Average RHIME and InTEM top-down seasonal emissions (solid lines) and 68% CI (dashed lines) with corresponding mean posterior sub-sector emissions are shown in (b) and (c), respectively.

As shown in Fig. 5, there are clear differences between the average bottom-up and top-down seasonal cycles for U.K. N_2O emissions across 2013-2022. To investigate what could be driving these differences, we use Bayesian inference (Section 2.5) to calculate scale factors for each UKEM sub-sector that optimize the fit to the observed average seasonal cycle. The seasonal profiles of the individual sectors from the UKEM are preserved.

Figure 7b and c show the optimized (posterior) sub-sectors that produce the best match with the derived seasonal cycles from RHIME and InTEM, respectively. We find the optimized fits do not generally have good agreement with the RHIME ($R^2 = 0.86$, $p < 0.01$) and InTEM ($R^2 = 0.11$, $p = 0.7$) seasonal cycles. Despite the large uncertainties in RHIME and InTEM there are certain months where the optimized bottom-up seasonal cycle does not fall within the RHIME/InTEM uncertainty. The fit to InTEM is generally worse than for RHIME, which could be due to the absence of two peaks in its average seasonal cycle and larger uncertainties than RHIME.

However for both RHIME and InTEM, a decrease in synthetic fertilizer emissions and an increase in "Other" emissions are inferred in the posterior seasonal profiles (Fig. 7, Table 2). An increase in emissions related to cattle manure during times of grazing and the spreading of poultry manure could explain some of the seasonal differences with RHIME-inferred emissions in the latter half of the year. Whereas an increase in emissions related to the spreading of digestate, cattle manure during times of grazing and housing could explain seasonal differences with InTEM-inferred emissions for the latter half of the year.

For January to April, there are only small differences between the RHIME/InTEM and optimized UKEM sub-sector emissions. After April, there is a larger mismatch be-

Table 2. Mean and 1σ uncertainty in the posterior scale factors for each UKEM emissions sub-sector when optimised to the average InTEM and RHIME seasonal cycles.

UKEM emissions sub-sector	InTEM-optimized scale factor	RHIME-optimized scale factor
Cattle manure, grazing	3.19 ± 1.61	5.12 ± 1.51
Cattle manure, housing	0.87 ± 0.87	0.05 ± 0.56
Cattle manure, spreading	1.83 ± 1.59	1.26 ± 1.28
Synthetic fertilizer	0.11 ± 0.20	0.17 ± 0.12
Spreading of digestate	1.11 ± 1.73	1.00 ± 1.70
Poultry manure, spreading	1.64 ± 1.73	3.41 ± 1.53
Other	2.05 ± 0.49	3.05 ± 0.43

tween these seasonal cycles. This mismatch could be attributed to retaining the seasonal profiles of each UKEM emissions sub-sectors, which could have time-correlated uncertainties.

4 Discussion

Continuous atmospheric N_2O measurements from the U.K. and Republic of Ireland were used in InTEM and RHIME inverse models to derive top-down U.K. N_2O emissions estimates and their trends over 2013-2022. Mean posterior U.K. terrestrial emissions from InTEM and RHIME over 2013-2022 were $90.5 \pm 23.0 (1\sigma)$ Gg N_2O yr^{-1} and $111.7 \pm 32.1 (1\sigma)$ Gg N_2O yr^{-1}, respectively. The two inversion systems inferred negative trends of -0.68 ± 0.48 Gg N_2O yr^{-2} and -2.10 ± 0.72 Gg N_2O yr^{-2}, respectively. However, it is unclear what could be driving a negative trend in the top-down emissions as the NAEI and UKEM sub-sector estimates do not have statistically significant trends over this period.

We find that the top-down emissions are close to the 2012-2014 U.K. emissions estimates of 101 (68-150) Gg N_2O yr^{-1} reported by Ganesan et al. (2015) and are approximately $14 - 33\%$ higher than the bottom-up N_2O emissions reported in NAEI. This discrepancy is similar to the $13-22\%$ differences between previously reported top-down and bottom-up estimates for the U.K. (Ganesan et al., 2015; Manning et al., 2011). However, we find the inventory emissions estimates are lower than the top-down estimates whereas previous U.K. N_2O studies found inventory emissions were higher. The U.K. emissions inventory updates the entire record each year. Revisions to the U.K.'s N_2O emissions are reflected in the U.K.'s NIR submitted to the UNFCCC, which, for 2022, reported smaller N_2O emissions than were used as the a priori estimates in Ganesan et al. (2015) and Manning et al. (2011) at the time. Average differences of $14 - 33\%$ between top-down and bottom-up U.K. N_2O emissions underscore that there are still large uncertainties in U.K. N_2O emissions.

Similar to previous regional N_2O studies (e.g. Ganesan et al., 2015; Nevison et al., 2018; Wagner-Riddle et al., 2017; Jeong et al., 2012) we observe a pronounced seasonal cycle in the top-down N_2O emissions with a large springtime peak. We also observe a secondary peak in the late summer and/or a prolonged decay in the spring peak, which have not been previously observed in the U.K. The observed seasonal patterns are likely to be driven by agricultural sources since the timings of these peaks are broadly consistent each year but climatic patterns could also have an influence. Top-down N_2O emissions estimates in California, USA suggest the higher N_2O emissions observed during spring are linked to the application of fertilizers (Jeong et al., 2018, 2012; Xiang et al., 2013).

Nevison et al. (2018) observed a dual seasonal maxima in top-down emissions from 2008-2014 in the USA with a spring peak attributed to fertilizer applications and a late winter peak attributed to freeze-thaw effects (e.g. Wagner-Riddle et al., 2017). Higher average winter temperatures in the U.K. and the timing of the second peak make it unlikely for freeze-thaw effects to be a driver of seasonal variations of N_2O emissions in the U.K. Recent N_2O flux measurements over different terrestrial ecosystems in the U.K. found inconsistent seasonal patterns of total N_2O emissions across different land use types (Sgouridis & Ullah, 2017). This further suggests that seasonal variations with a springtime peak previously observed in the U.K. are driven by agricultural sources. However, environmental drivers such as precipitation and surface temperature also influence the magnitude and timing of agricultural N_2O emissions (Skiba et al., 2012).

We find the agreement between the average top-down and bottom-up seasonal cycles could be improved by reducing UKEM synthetic fertilizer N_2O emissions by an average factor of 0.15±0.12 and increasing N_2O emissions from certain types of manure management - spreading of digestate and cattle manure during times of grazing and cattle housing - by an average factor of 4.2±1.5. Modelling the temporal changes of manure management N_2O emissions is challenging as livestock waste management systems vary between sites and over time with little information available about their management practices (Chang et al., 2004). However, it is also possible the top-down and bottom-up seasonal cycle mismatch could be attributed to several other sources - such as missing emissions from NH_3 deposition - but this requires further investigation.

Whilst we find top-down emissions from InTEM and RHIME are well-correlated ($R^2 = 0.86$, $p < 0.01$) there are differences in the magnitude and seasonal variations of N_2O emissions and uncertainties. Discrepancies between InTEM and RHIME potentially arise from differences in the calculation of boundary condition mole fractions, the treatment of model-data uncertainties and the approach for calculating posterior emissions in each inverse method. We find an average difference of 0.18±0.22(1σ) ppb between the boundary condition mole fractions (Text S4). A lower mole fraction baseline would lead to higher emissions being derived in the inversion.

The results from these long-term U.K. atmospheric N_2O measurements from a dense measurement network demonstrate that they can be used for effective evaluation of regional N_2O emissions by using inverse modelling. Understanding of differences between top-down and bottom-up N_2O emissions could be enhanced by comparing top-down emissions derived using a different atmospheric transport model with different underlying meteorological fields. Further long-term flux measurements of N_2O emissions sources could also provide additional constraints on the seasonal discrepancies observed between the average top-down and bottom-up seasonal cycles.

5 Conclusions

This study presents 10 years of top-down N_2O emissions derived using atmospheric measurements from across the U.K. and Republic of Ireland. Posterior emissions from both InTEM and RHIME inverse models find average U.K. emissions of 90.5±23.0 Gg N_2O yr^{-1} and 111.7 ± 32.1 Gg N_2O yr^{-1}, respectively across 2013-2020 which are ∼ 14.0 ± 41.0% and ∼ 32.7 ± 23.2% higher than estimated in the U.K. national atmospheric emissions inventory, respectively. Average differences between the top-down and UKEM bottom-up seasonal patterns could be explained by decreasing synthetic fertilizer emissions by an average factor of ∼ 0.15±0.12, and increasing N_2O manure management emissions (from cattle manure during grazing and housing) by an average factor of 4.2±1.5. However, we find large uncertainties associated with the posterior scaling factors for the agricultural seasonal emissions profiles.

6 Open Research

Atmospheric measurements of N_2O used in this work are available from the CEDA Archive (O'Doherty et al., 2020): `https://data.ceda.ac.uk/badc/uk-decc-network/data/n2o/v23.08`. A doi for this data is currently being assigned. Python scripts used for data analysis are available for use in `https://github.com/EricSaboya/uk_n2o`

Acknowledgments

ES, ALG and MR were supported by NERC Highlight Topic Detection and Attribution of Regional Emissions in the UK (DARE-UK, NE/S004211/1). Thank you to Ray Weiss and Chris Harth of SIO for providing the measurement calibration standards. Thank you to Esme Curtis for proofreading the article.

References

Arnold, T., Manning, A. J., Kim, J., Li, S., Webster, H., Thomson, D., ... O'Doherty, S. (2018). Inverse modelling of CF4 and NF3 emissions in East Asia. *Atmospheric Chemistry and Physics*, *18*(18), 13305–13320. doi: 10.5194/acp-18-13305-2018

Brown, P., Cardenas, L., Choudrie, S., Del Vento, S., Karagianni, E., MacCarthy, J., ... Wakeling, D. (2022). *UK Greenhouse Gas Inventory 1990 to 2020: Annual Report for submission under the Framework Convention on Climate Change* (Tech. Rep.).

Brown, P., Cardenas, L., Del Vento, S., Karagianni, E., MacCarthy, J., Mullen, P., ... Willis, D. (2023). *UK Greenhouse Gas Inventory, 1990 to 2021 Annual Report for Submission under the Framework Convention on Climate Change* (Tech. Rep.). UK Department for Energy Security and Net Zero.

Chang, Y. H., Scrimshaw, M. D., & Lester, J. N. (2004). *IPCC Good Practice Guidance and Uncertainty Management in National Greenhouse Gas Inventories* (Vol. 25; Tech. Rep. No. 2).

Committee on Climate Change. (2015). *The Fifth Carbon Budget: The next step towards a low-carbon economy* (Tech. Rep.). Retrieved from `https://www.theccc.org.uk/publication/the-fifth-carbon-budget-the-next-step-towards-a-low-carbon-economy/`

Crippa, M., Guizzardi, D., Solazzo, E., Muntean, M., Schaaf, E., Monforti-Ferrario, F., ... Vignati, E. (2021). *GHG emissions of all world countries - 2021 Report* (No. October).

Ganesan, A. L., Manizza, M., Morgan, E. J., Harth, C. M., Kozlova, E., Lueker, T., ... Rigby, M. (2020). Marine Nitrous Oxide Emissions From Three Eastern Boundary Upwelling Systems Inferred From Atmospheric Observations. *Geophysical Research Letters*, *47*(14). doi: 10.1029/2020GL087822

Ganesan, A. L., Manning, A. J., Grant, A., Young, D., Oram, D. E., Sturges, W. T., ... O'Doherty, S. (2015, 6). Quantifying methane and nitrous oxide emissions from the UK and Ireland using a national-scale monitoring network. *Atmospheric Chemistry and Physics*, *15*(11), 6393–6406. Retrieved from `https://acp.copernicus.org/articles/15/6393/2015/` doi: 10.5194/acp-15-6393-2015

Ganesan, A. L., Rigby, M., Zammit-Mangion, A., Manning, A. J., Prinn, R. G., Fraser, P. J., ... Weiss, R. F. (2014). Characterization of uncertainties in atmospheric trace gas inversions using hierarchical Bayesian methods. *Atmospheric Chemistry and Physics*, *14*(8). doi: 10.5194/acp-14-3855-2014

Hall, B. D., Dutton, G. S., & Elkins, J. W. (2007). The NOAA nitrous oxide standard scale for atmospheric observations. *Journal of Geophysical Research Atmospheres*, *112*(9). doi: 10.1029/2006JD007954

Hoffman, M. D., & Gelman, A. (2014). The no-U-turn sampler: Adaptively set-

ting path lengths in Hamiltonian Monte Carlo. *Journal of Machine Learning Research*, *15*.

Jeong, S., Newman, S., Zhang, J., Andrews, A. E., Bianco, L., Dlugokencky, E., ... Fischer, M. L. (2018). Inverse Estimation of an Annual Cycle of California's Nitrous Oxide Emissions. *Journal of Geophysical Research: Atmospheres*, *123*(9). doi: 10.1029/2017JD028166

Jeong, S., Zhao, C., Andrews, A. E., Dlugokencky, E. J., Sweeney, C., Bianco, L., ... Fischer, M. L. (2012). Seasonal variations in N2O emissions from central California. *Geophysical Research Letters*, *39*(16). doi: 10.1029/2012GL052307

Jones, A., Thomson, D., Hort, M., & Devenish, B. (2007, 4). The U.K. Met Office's Next-Generation Atmospheric Dispersion Model, NAME III. In *Air pollution modeling and its application xvii* (pp. 580–589). Springer US. doi: 10.1007/978-0-387-68854-1{_}62

Lessin, G., Polimene, L., Artioli, Y., Butenschön, M., Clark, D. R., Brown, I., & Rees, A. P. (2020). Modeling the Seasonality and Controls of Nitrous Oxide Emissions on the Northwest European Continental Shelf. *Journal of Geophysical Research: Biogeosciences*, *125*(6). doi: 10.1029/2019JG005613

Levy, P. (2020). *Greenhouse Gas Fluxes from the UK (ukghg).* Retrieved from `https://github.com/NERC-CEH/ukghg/blob/`

Levy, P. E., Cowan, N., van Oijen, M., Famulari, D., Drewer, J., & Skiba, U. (2017). Estimation of cumulative fluxes of nitrous oxide: uncertainty in temporal upscaling and emission factors. *European Journal of Soil Science*, *68*(4). doi: 10.1111/ejss.12432

Lunt, M. F., Manning, A. J., Allen, G., Arnold, T., Bauguitte, S. J.-B., Boesch, H., ... Rigby, M. (2021, 11). Atmospheric observations consistent with reported decline in the UK's methane emissions (2013–2020). *Atmospheric Chemistry and Physics*, *21*(21), 16257–16276. Retrieved from `https://acp.copernicus.org/articles/21/16257/2021/` doi: 10.5194/acp-21-16257-2021

Manning, A. J., O'Doherty, S., Jones, A. R., Simmonds, P. G., & Derwent, R. G. (2011). Estimating UK methane and nitrous oxide emissions from 1990 to 2007 using an inversion modeling approach. *Journal of Geophysical Research Atmospheres*, *116*(2), 1–19. doi: 10.1029/2010JD014763

Manning, A. J., Redington, A. L., Say, D., O'Doherty, S., Young, D., Simmonds, P. G., ... Arnold, T. (2021). Evidence of a recent decline in UK emissions of hydrofluorocarbons determined by the InTEM inverse model and atmospheric measurements. *Atmospheric Chemistry and Physics*, *21*(16), 12739–12755. doi: 10.5194/acp-21-12739-2021

Nevison, C., Andrews, A., Thoning, K., Dlugokencky, E., Sweeney, C., Miller, S., ... Nehrkorn, T. (2018). Nitrous Oxide Emissions Estimated With the CarbonTracker-Lagrange North American Regional Inversion Framework. *Global Biogeochemical Cycles*, *32*(3). doi: 10.1002/2017GB005759

O'Doherty, S., Say, D., Stanley, K., Spain, G., Arnold, T., Rennick, C., ... Grant, A. (2020). *UK DECC (Deriving Emissions linked to Climate Change) Network. Centre for Environmental Data Analysis.* Retrieved from `http://catalogue.ceda.ac.uk/uuid/f5b38d1654d84b03ba79060746541e4f`

Prinn, R. G., Weiss, R. F., Arduini, J., Arnold, T., Langley Dewitt, H., Fraser, P. J., ... Zhou, L. (2018). History of chemically and radiatively important atmospheric gases from the Advanced Global Atmospheric Gases Experiment (AGAGE). *Earth System Science Data*, *10*(2). doi: 10.5194/essd-10-985-2018

Redington, A. L., Manning, A. J., Henne, S., Graziosi, F., Western, L. M., Arduini, J., ... Young, D. (2023, 7). Western European emission estimates of CFC-11, CFC-12 and CCl4 derived from atmospheric measurements from 2008 to 2021. *Atmospheric Chemistry and Physics*, *23*(13), 7383–7398. doi: 10.5194/acp-23-7383-2023

Ricardo Energy & Environment. (2019). UK Emission Mapping Methodology 2017. (1), 49.

Rigby, M., Manning, A. J., & Prinn, R. G. (2012). The value of high-frequency, high-precision methane isotopologue measurements for source and sink estimation. *Journal of Geophysical Research Atmospheres*, *117*(12), 1–14. doi: 10.1029/2011JD017384

Rigby, M., Park, S., Saito, T., Western, L. M., Redington, A. L., Fang, X., ... Young, D. (2019). Increase in CFC-11 emissions from eastern China based on atmospheric observations. *Nature*, *569*(7757). doi: 10.1038/s41586-019-1193-4

Say, D., Manning, A. J., Western, L. M., Young, D., Wisher, A., Rigby, M., ... O'Doherty, S. (2021). Global trends and European emissions of tetrafluoromethane (CF4), hexafluoroethane (C2F6) and octafluoropropane (C3F8). *Atmospheric Chemistry and Physics*, *21*(3). doi: 10.5194/acp-21-2149-2021

Sgouridis, F., & Ullah, S. (2017). Soil Greenhouse Gas Fluxes, Environmental Controls, and the Partitioning of N2O Sources in UK Natural and Seminatural Land Use Types. *Journal of Geophysical Research: Biogeosciences*, *122*(10). doi: 10.1002/2017JG003783

Skiba, U., Jones, S. K., Dragosits, U., Drewer, J., Fowler, D., Rees, R. M., ... Manning, A. J. (2012). *UK emissions of the greenhouse gas nitrous oxide* (Vol. 367) (No. 1593). doi: 10.1098/rstb.2011.0356

Stanley, K. M., Grant, A., O'Doherty, S., Young, D., Manning, A. J., Stavert, A. R., ... Derwent, R. G. (2018). Greenhouse gas measurements from a UK network of tall towers: Technical description and first results. *Atmospheric Measurement Techniques*, *11*(3), 1437–1458. doi: 10.5194/amt-11-1437-2018

Stavert, A. R., O'Doherty, S., Stanley, K., Young, D., Manning, A. J., Lunt, M. F., ... Arnold, T. (2019). UK greenhouse gas measurements at two new tall towers for aiding emissions verification. *Atmospheric Measurement Techniques*, *12*(8). doi: 10.5194/amt-12-4495-2019

Stell, A. C., Bertolacci, M., Zammit-Mangion, A., Rigby, M., Fraser, P. J., Harth, C. M., ... Ganesan, A. L. (2022). Modelling the growth of atmospheric nitrous oxide using a global hierarchical inversion. *Atmospheric Chemistry and Physics*, *22*(19). doi: 10.5194/acp-22-12945-2022

Thompson, R. L., Chevallier, F., Crotwell, A. M., Dutton, G., Langenfelds, R. L., Prinn, R. G., ... Aoki, S. (2014). Nitrous oxide emissions 1999 to 2009 from a global atmospheric inversion. *Atmospheric Chemistry and Physics*, *14*(4). doi: 10.5194/acp-14-1801-2014

Thompson, R. L., Gerbig, C., & Rödenbeck, C. (2011). A Bayesian inversion estimate of N2O emissions for western and central Europe and the assessment of aggregation errors. *Atmospheric Chemistry and Physics*, *11*(7). doi: 10.5194/acp-11-3443-2011

Thompson, R. L., Lassaletta, L., Patra, P. K., Wilson, C., Wells, K. C., Gressent, A., ... Canadell, J. G. (2019). Acceleration of global N2O emissions seen from two decades of atmospheric inversion. *Nature Climate Change*, *9*(12). doi: 10.1038/s41558-019-0613-7

Tian, H., Xu, R., Canadell, J. G., Thompson, R. L., Winiwarter, W., Suntharalingam, P., ... Yao, Y. (2020). A comprehensive quantification of global nitrous oxide sources and sinks. *Nature*, *586*(7828). doi: 10.1038/s41586-020-2780-0

UK Department for Business Energy and Industrial Strategy. (2022). *Updated energy and emissions projections 2021 to 2040* (Tech. Rep.). Retrieved from `https://www.gov.uk/government/publications/energy-and-emissions-projections-2021-to-2040`

U.K. Department for Energy Security and Net Zero. (2022). *Energy and emissions projections: 2021 to 2040* (Tech. Rep.). Retrieved from `https://www.gov.uk/government/publications/energy-and-emissions-projections-2021-to`

-2040

UK Government. (2008). *Climate Change Act 2008: Elizabeth II. Chapter 27.*

Wagner-Riddle, C., Congreves, K. A., Abalos, D., Berg, A. A., Brown, S. E., Ambadan, J. T., ... Tenuta, M. (2017). Globally important nitrous oxide emissions from croplands induced by freeze-thaw cycles. *Nature Geoscience*, *10*(4). doi: 10.1038/ngeo2907

Wells, K. C., Millet, D. B., Bousserez, N., Henze, D. K., Griffis, T. J., Chaliyakunnel, S., ... Paul Steele, L. (2018). Top-down constraints on global N2O emissions at optimal resolution: Application of a new dimension reduction technique. *Atmospheric Chemistry and Physics*, *18*(2). doi: 10.5194/acp-18-735-2018

Western, L. M., Redington, A. L., Manning, A. J., Trudinger, C. M., Hu, L., Henne, S., ... Rigby, M. (2022, 7). A renewed rise in global HCFC-141b emissions between 2017-2021. *Atmospheric Chemistry and Physics*, *22*(14), 9601–9616. doi: 10.5194/acp-22-9601-2022

Xiang, B., Miller, S. M., Kort, E. A., Santoni, G. W., Daube, B. C., Commane, R., ... Wofsy, S. C. (2013). Nitrous oxide (N2O) emissions from California based on 2010 CalNex airborne measurements. *Journal of Geophysical Research Atmospheres*, *118*(7). doi: 10.1002/jgrd.50189

Figure 1.

Total

10°W 5°W 0°

60°N (a)

55°N

50°N

0 0.2 0.4 0.6 0.8 1.0

N_2O emissions (Mg N_2O yr^{-1})

Agriculture

10°W 5°W 0°

60°N (b)

55°N

50°N

0 0.2 0.4 0.6 0.8 1.0

N_2O emissions (Mg N_2O yr^{-1})

Other

10°W 5°W 0°

60°N (c)

55°N

50°N

0 0.2 0.4 0.6 0.8 1.0

N_2O emissions (Mg N_2O yr^{-1})

Marine

10°W 5°W 0°

60°N (d)

55°N

50°N

0 0.02 0.04 0.06 0.08 0.1

N_2O emissions (Mg N_2O yr^{-1})

Figure 2.

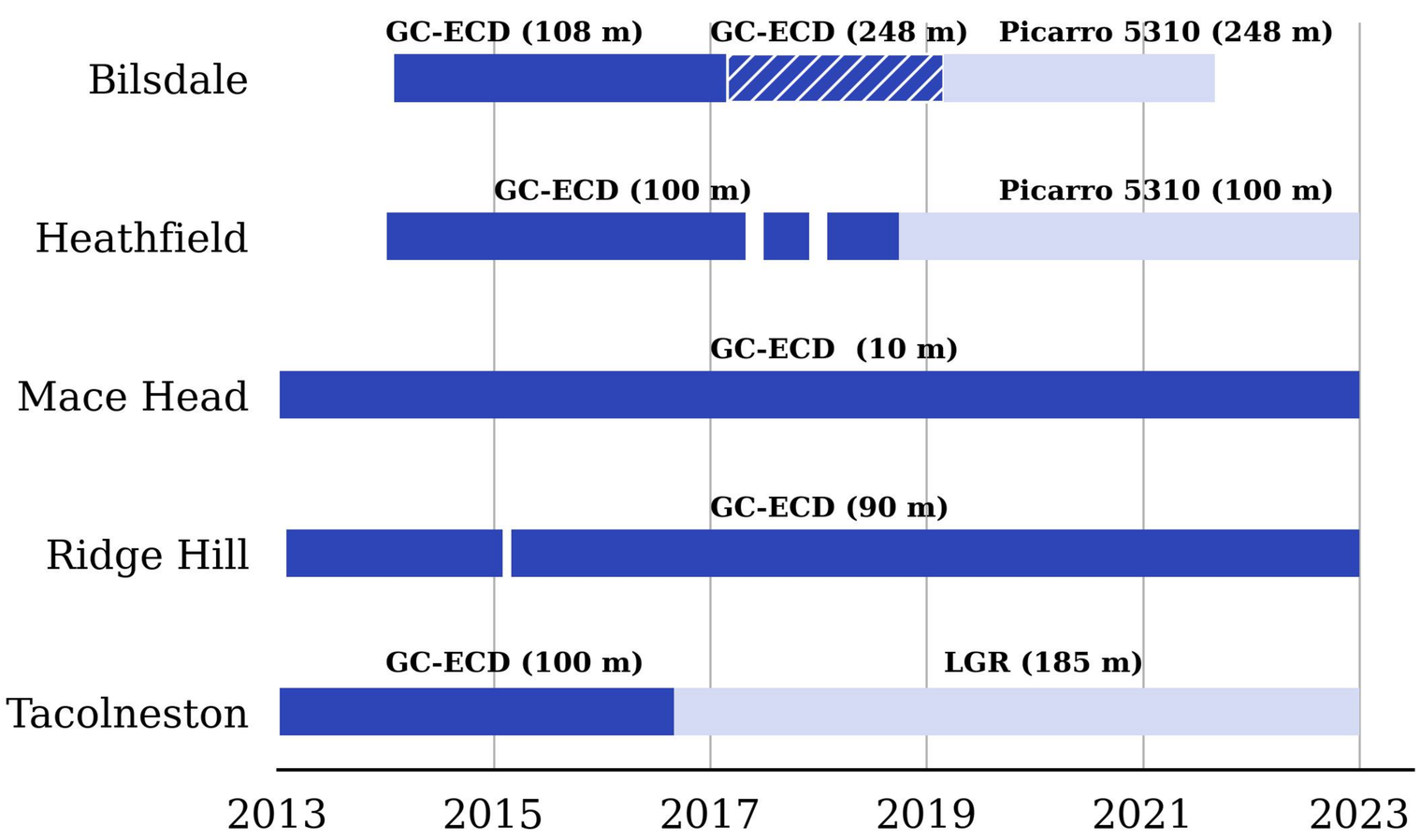
GC-ECD (108 m)
GC-ECD (248 m)
Picarro 5310 (248 m)
Bilsdale
GC-ECD (100 m)
Picarro 5310 (100 m)
Heathfield
GC-ECD (10 m)
Mace Head
GC-ECD (90 m)
Ridge Hill
GC-ECD (100 m)
LGR (185 m)
Tacolneston
2013
2015
2017
2019
2021
2023

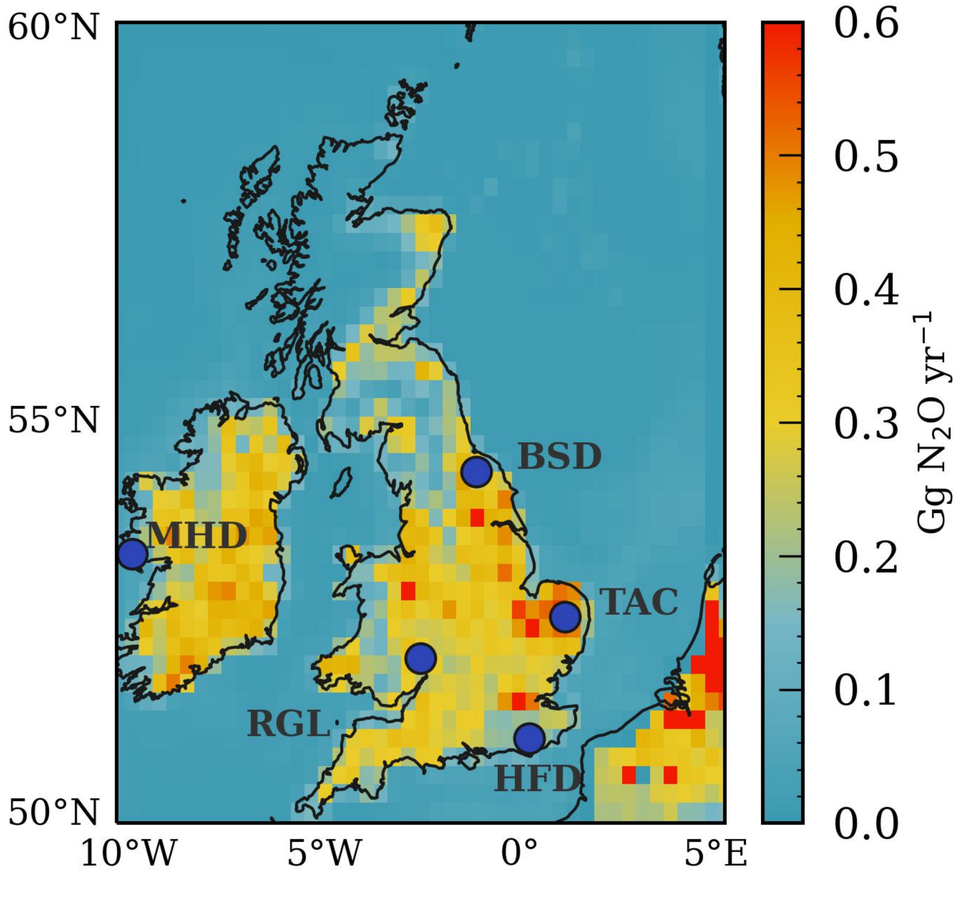
60°N
55°N
50°N
10°W
5°W
0°
5°E
BSD
MHD
TAC
RGL
HFD
0.6
0.5
0.4
0.3
0.2
0.1
0.0
Gg N2O yr−1

Figure 3.

(a)

Monthly prior (land + sea)
Monthly prior (land)
InTEM (land + sea)
InTEM (land)
RHIME (land + sea)
RHIME (land)

U.K. N_2O emissions (Gg N_2O yr^{-1})

250
200
150
100
50
0

2013 2014 2015 2016 2017 2018 2019 2020 2021 2022 2023

Year

(b)

Monthly prior (land)
Annual prior (land)
InTEM (monthly prior)
InTEM (annual prior)
RHIME (land)
RHIME (annual prior)

U.K. N_2O emissions (Gg N_2O yr^{-1})

250
200
150
100
50
0

2013 2014 2015 2016 2017 2018 2019 2020 2021 2022 2023

Year

Figure 4.

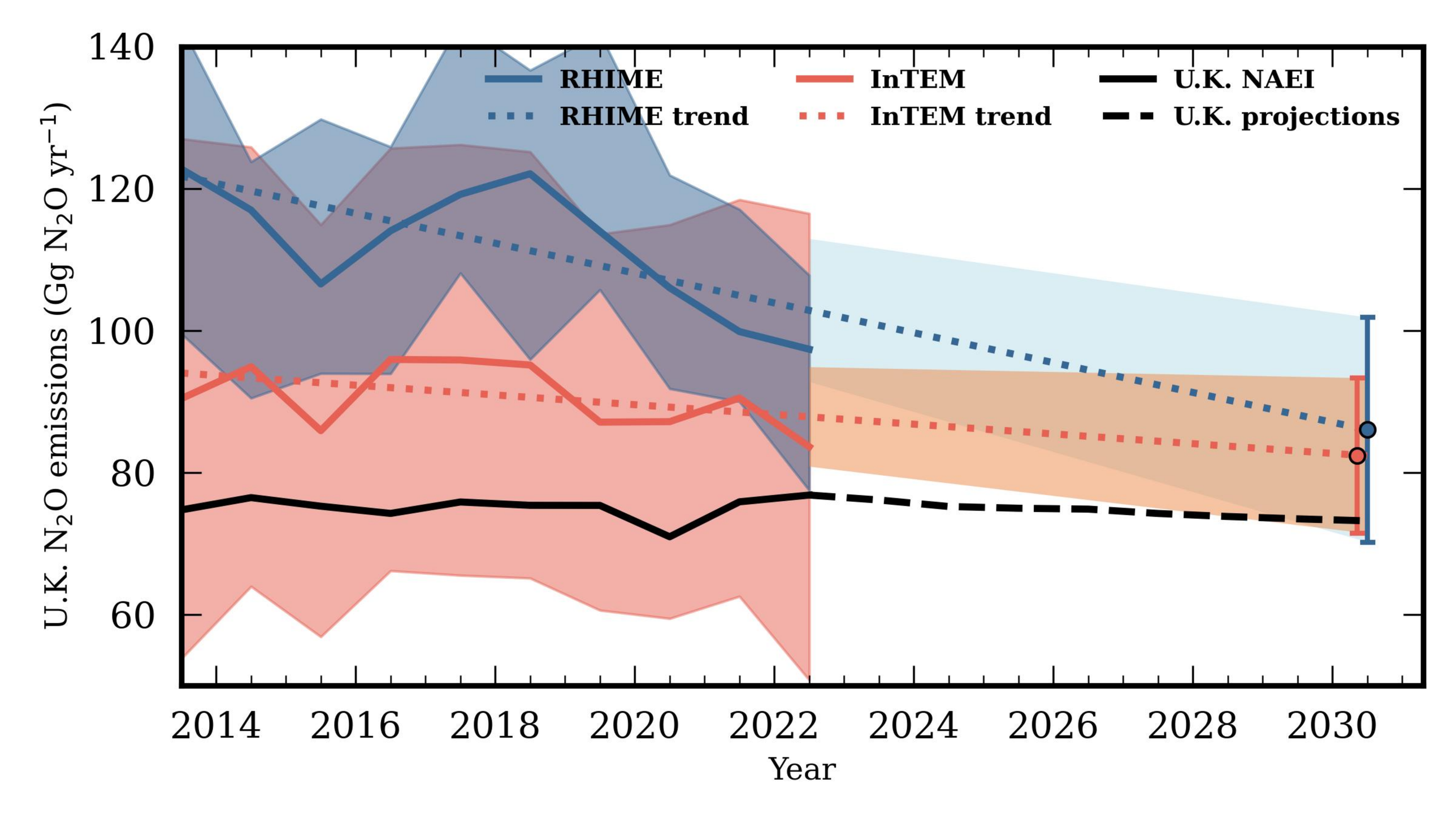
RHIME
RHIME trend
InTEM
InTEM trend
U.K. NAEI
U.K. projections
U.K. N_2O emissions (Gg N_2O yr^{-1})
140
120
100
80
60
2014
2016
2018
2020
2022
2024
2026
2028
2030
Year

Figure 5.

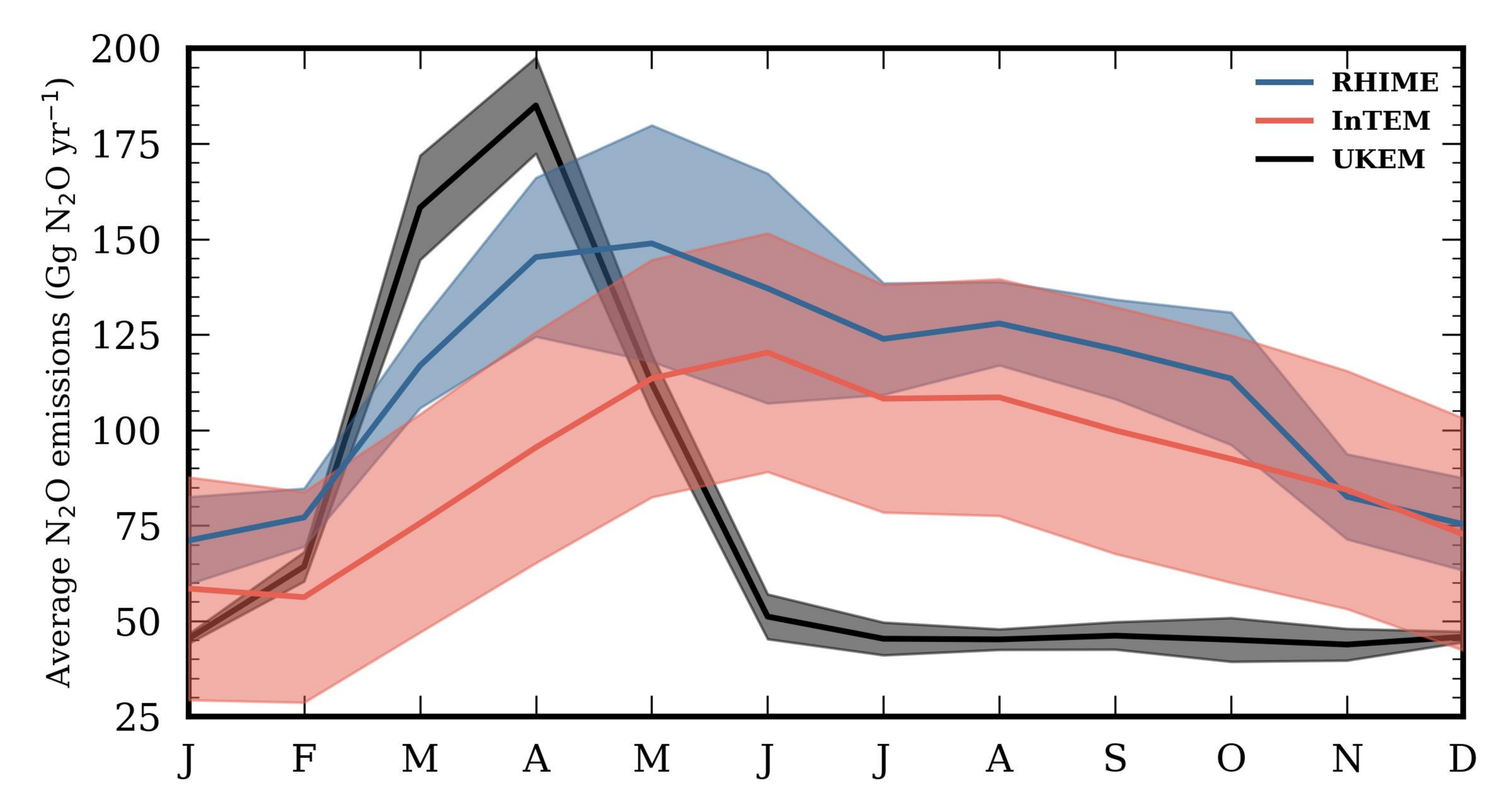
RHIME
InTEM
UKEM
Average N_2O emissions (Gg N_2O yr^{-1})
200
175
150
125
100
75
50
25
J
F
M
A
M
J
J
A
S
O
N
D

Figure 6.

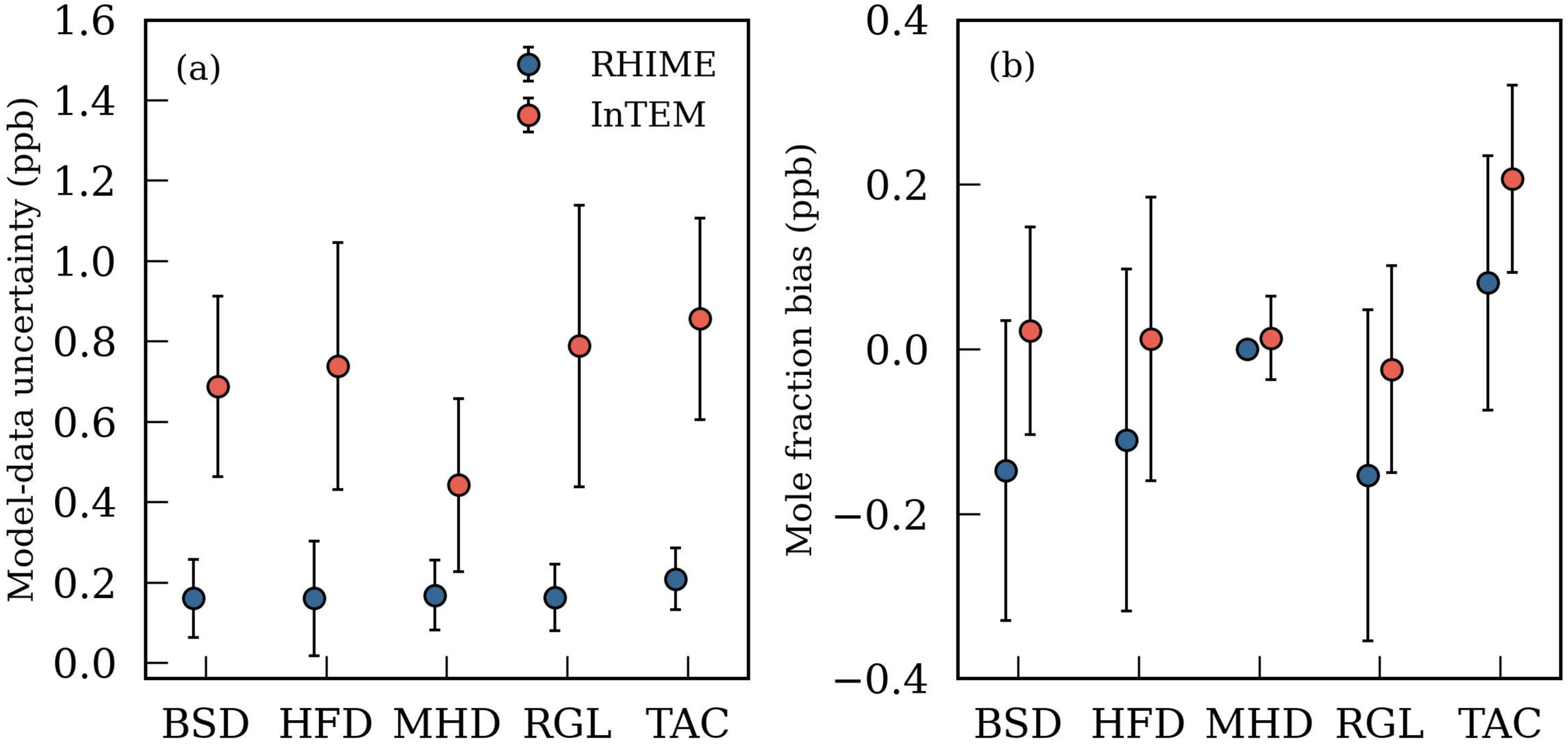
(a)
RHIME
InTEM
Model-data uncertainty (ppb)
1.6
1.4
1.2
1.0
0.8
0.6
0.4
0.2
0.0
BSD
HFD
MHD
RGL
TAC
(b)
Mole fraction bias (ppb)
0.4
0.2
0.0
−0.2
−0.4
BSD
HFD
MHD
RGL
TAC

Figure 7.

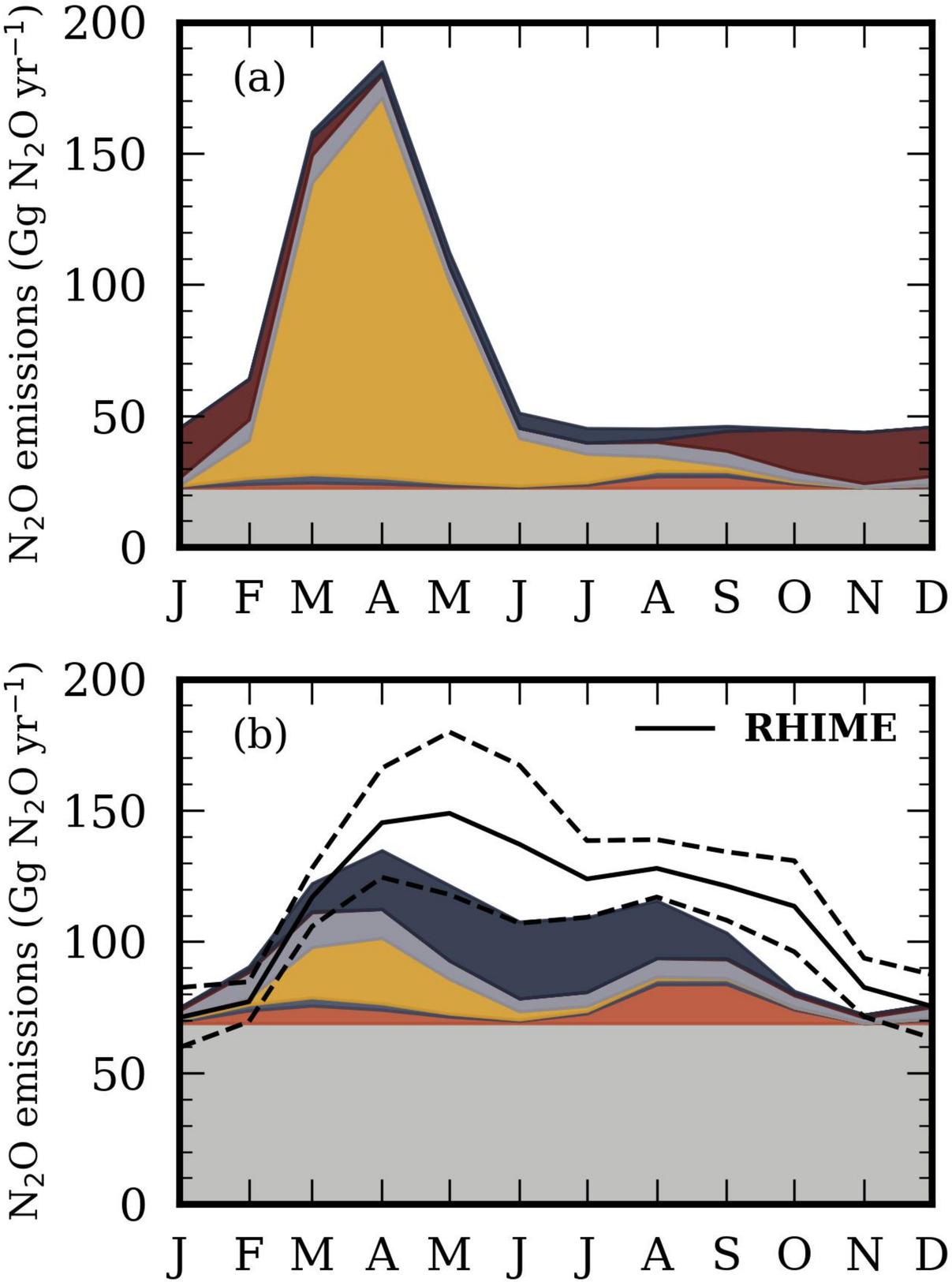
(a)
(b)
RHIME
(c)
InTEM
N_2O emissions (Gg N_2O yr^{-1})
0
50
100
150
200
J F M A M J J A S O N D

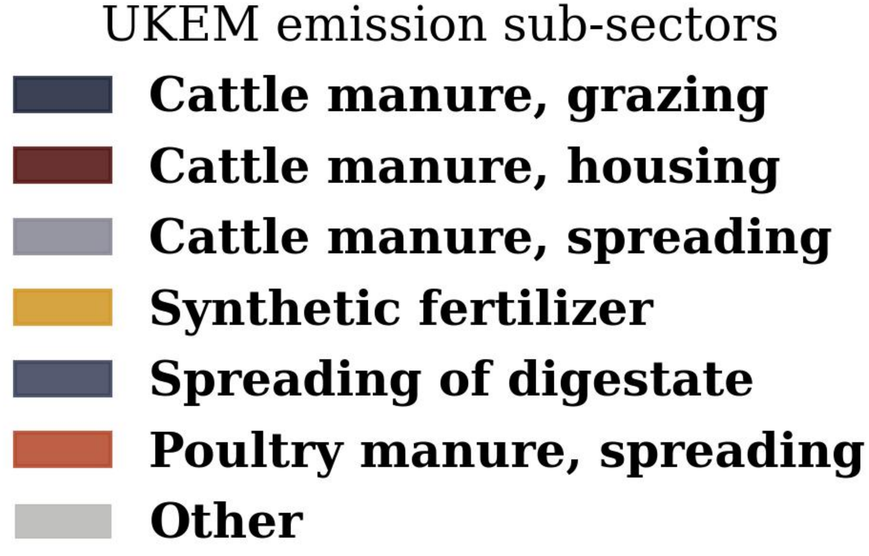
UKEM emission sub-sectors
Cattle manure, grazing
Cattle manure, housing
Cattle manure, spreading
Synthetic fertilizer
Spreading of digestate
Poultry manure, spreading
Other

Figure S1.

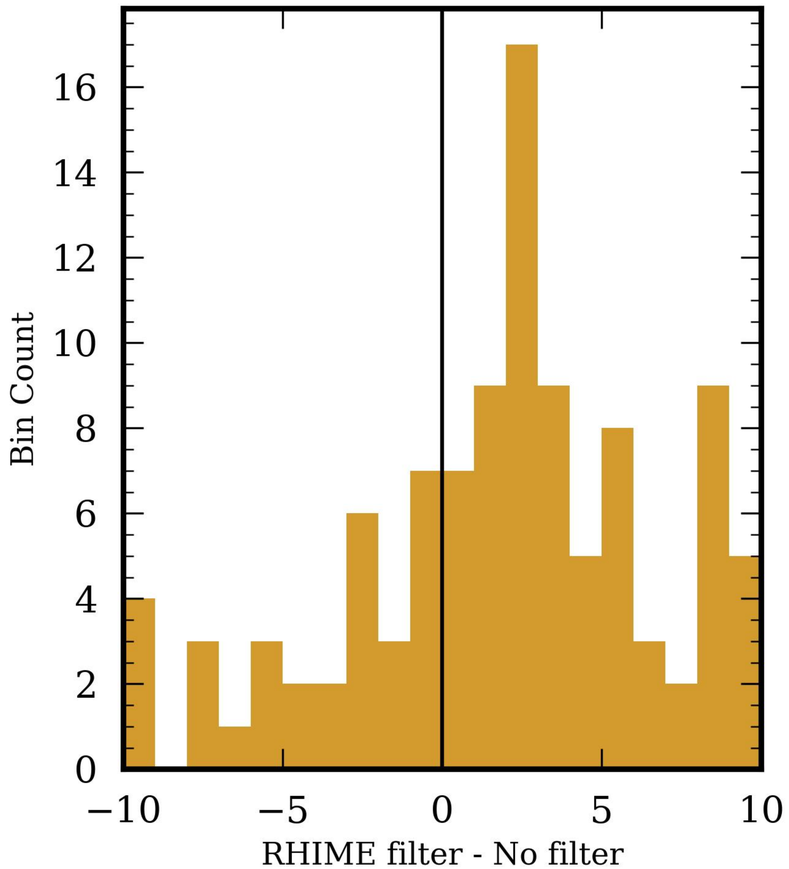
Bin Count
RHIME filter - No filter

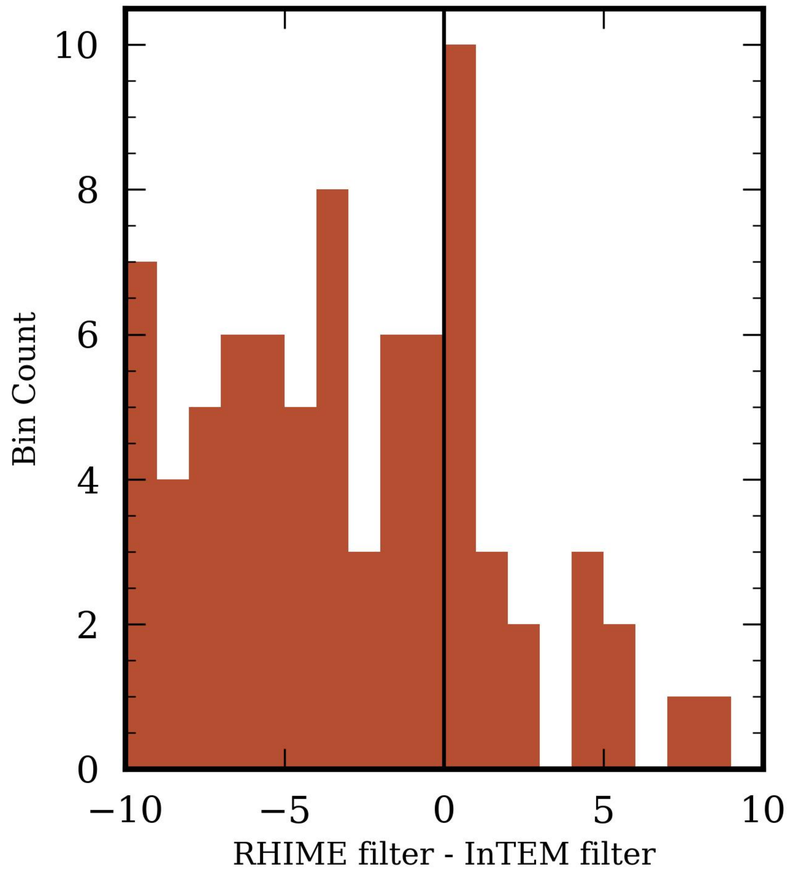
Bin Count
RHIME filter - InTEM filter

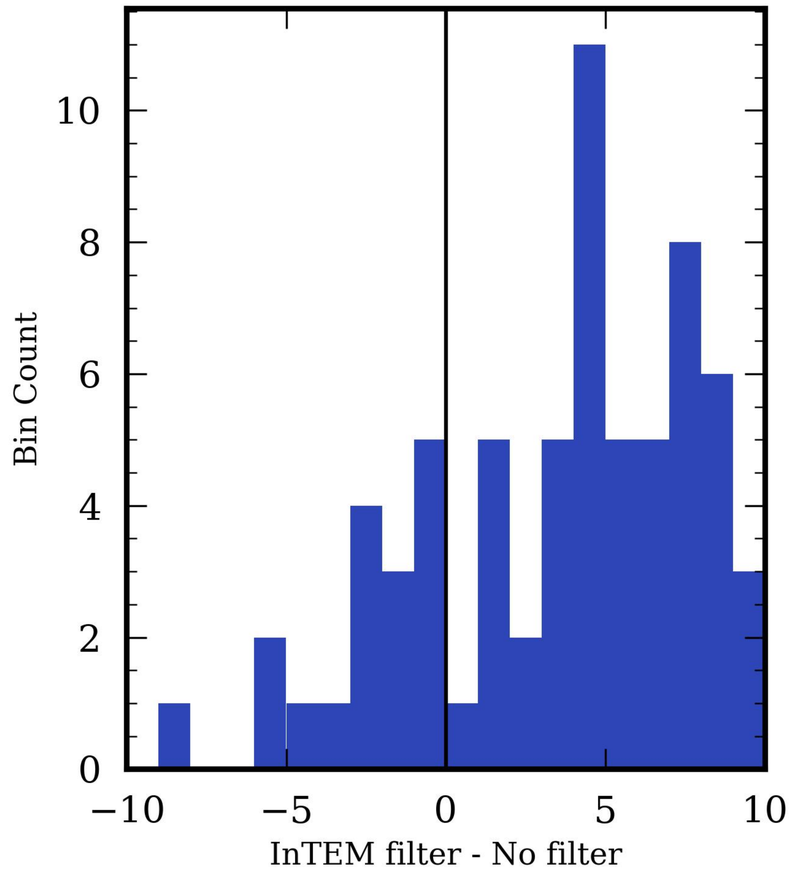
Bin Count
InTEM filter - No filter

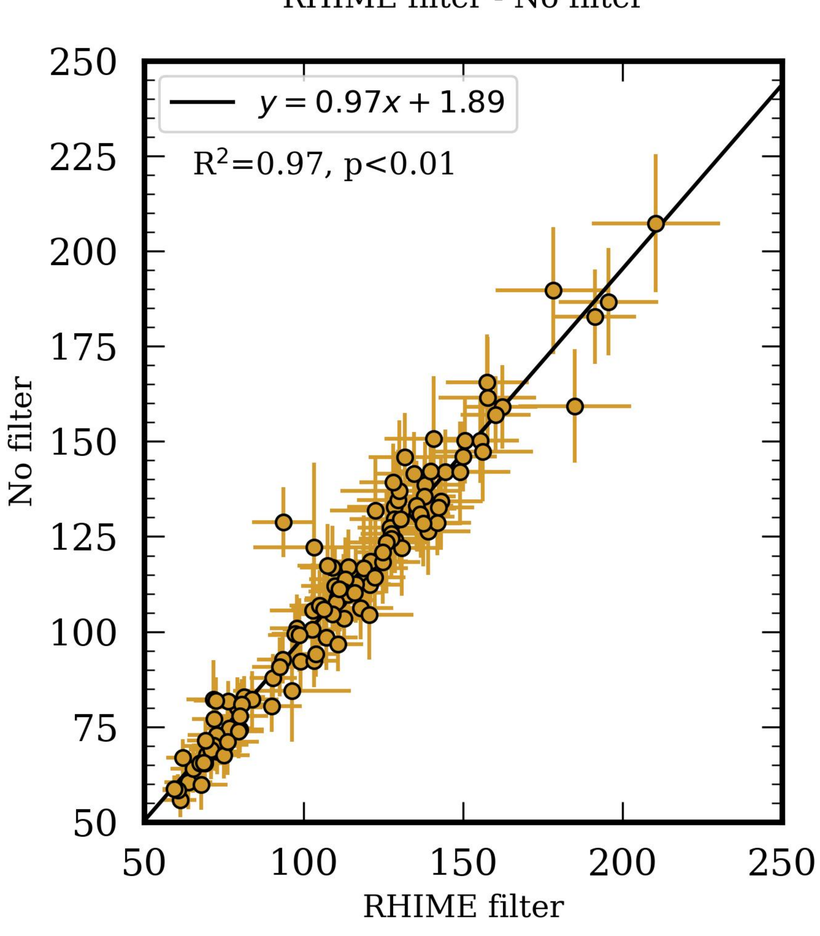
y = 0.97x + 1.89
R²=0.97, p<0.01
No filter
RHIME filter

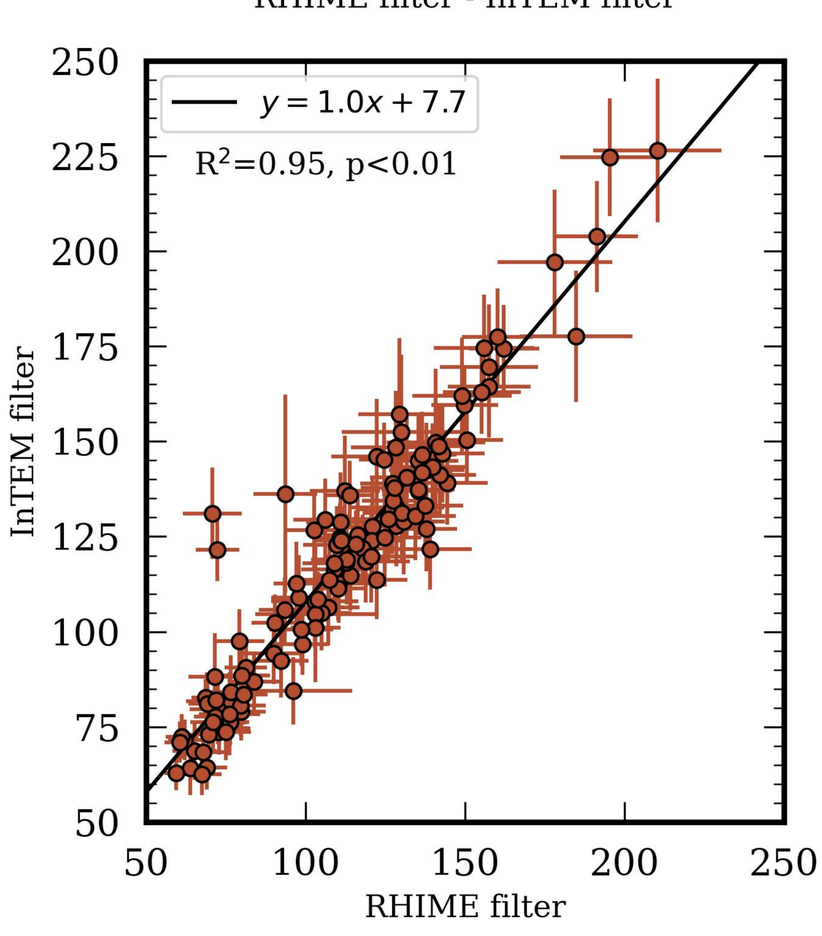
y = 1.0x + 7.7
R²=0.95, p<0.01
InTEM filter
RHIME filter

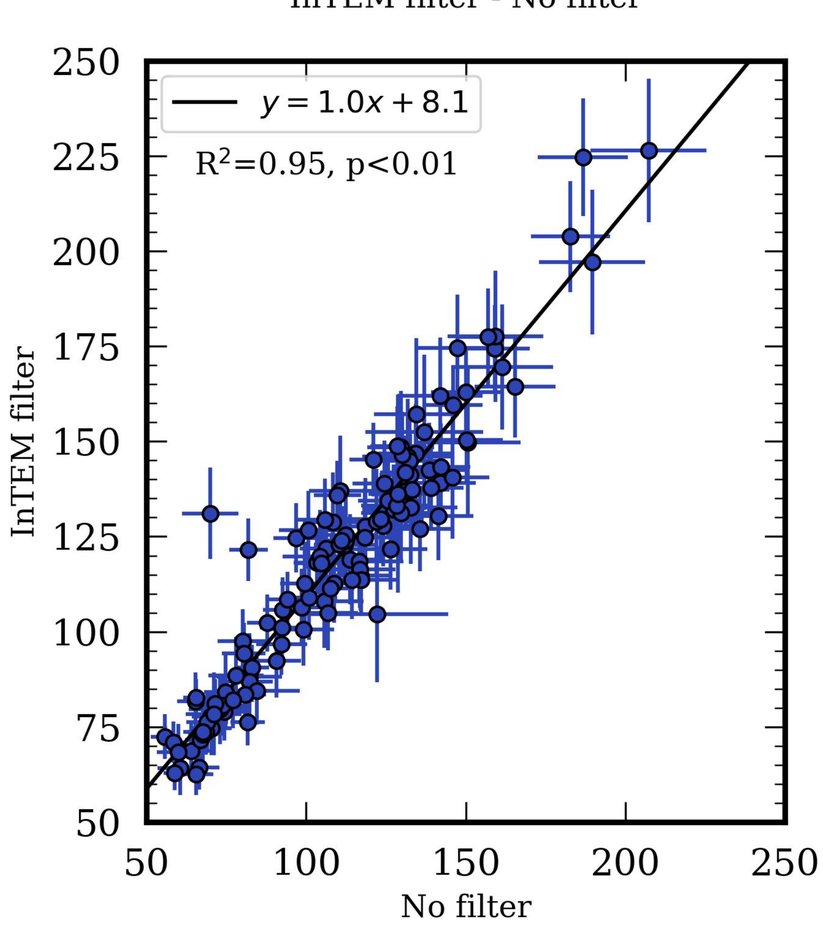
y = 1.0x + 8.1
R²=0.95, p<0.01
InTEM filter
No filter

Figure S2.

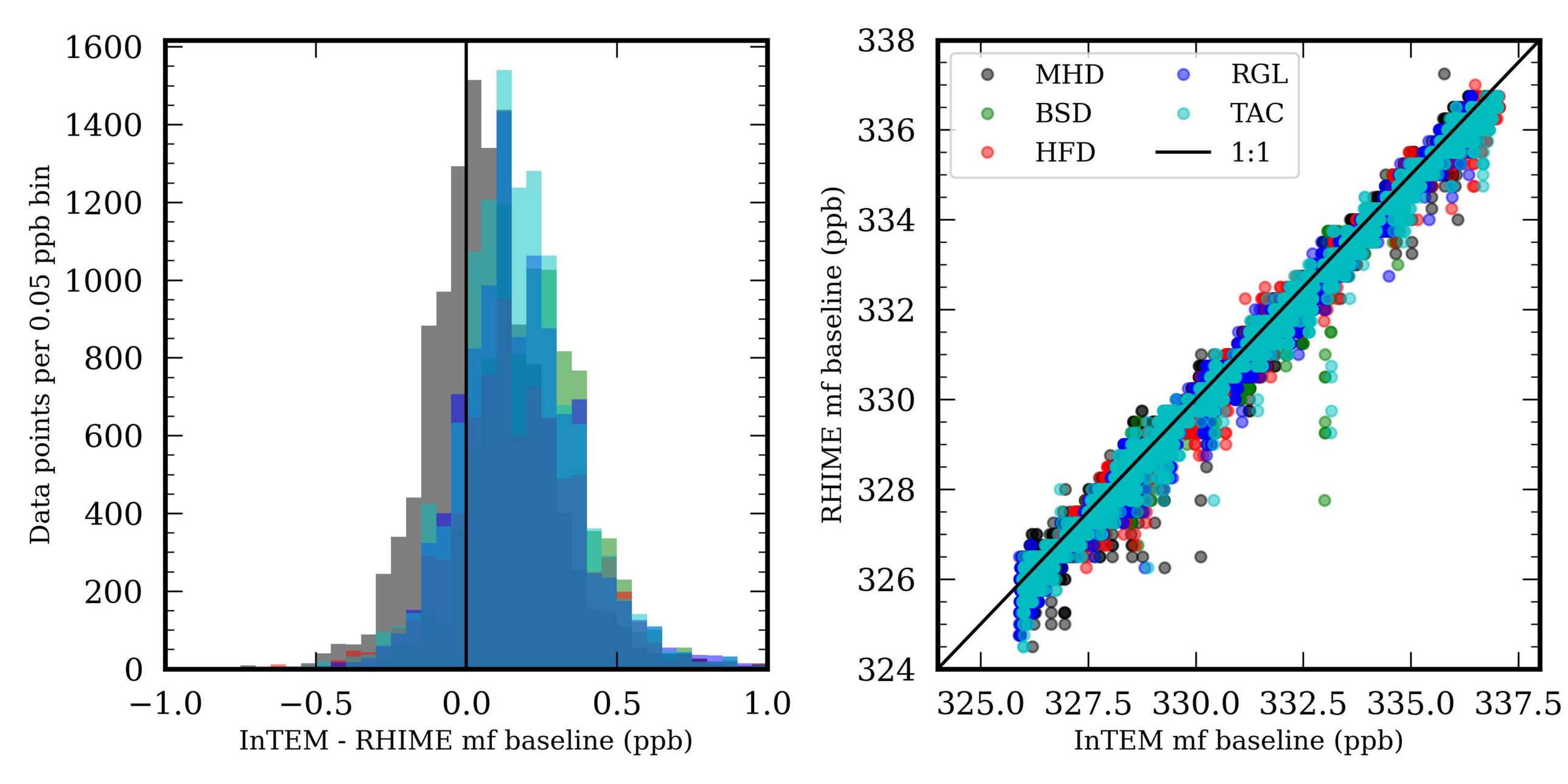
Data points per 0.05 ppb bin
InTEM - RHIME mf baseline (ppb)
RHIME mf baseline (ppb)
InTEM mf baseline (ppb)
MHD
BSD
HFD
RGL
TAC
1:1